Wind Farm Design

Strategy-based IMAP optimization for parametrically scalable offshore wind farm design

N.H.M. (Niels) Roeders

Technische Universiteit Delft

Wind Farm Design

Strategy-based IMAP optimization for parametrically scalable offshore wind farm design

by

N.H.M. (Niels) Roeders

to obtain the degree of Master of Science,

in the field of Civil Engineering,

at the Delft University of Technology,

to be defended publicly on 12-07-2024 at 13:45

Student number:	4871006	
Project duration:	February 9, 2024 – July 12, 2024	
Thesis committee:	J.O. Colomés Gene,	TU Delft, Chairman Committee
	S. van Nederveen,	TU Delft, Comittee Member
	M. Capaldo,	TotalEnergies, Company supervisor
	Z. Allybokus,	TotalEnergies, Company supervisor
	M. Rondon	TotalEnergies, Company supervisor

*This thesis is confidential and cannot be made public until **12-07-2026***

An electronic version of this thesis work is available at: `http://repository.tudelft.nl/`.

[**Cover: Egmond aan Zee Offshore Wind Farm by Deltares**].

The work in this thesis was supported by TotalEnergies
Their cooperation is hereby gratefully acknowledged.

Preface

As I approach the completion of my Master's degree in Civil Engineering at TU Delft, with a focus on hydraulic and offshore structures, I reflect on the journey that has led to this thesis. This work is the result of a collaborative effort between TU Delft and TotalEnergies, carried out within the innovative environment of the TotalEnergies R&D wind department in Paris, France.
The goal of this research was to improve on the complex challenge of optimizing offshore wind farms, a task that is crucial for the advancement of sustainable energy. The support and expertise provided by both academic and industry professionals have been invaluable in guiding this project towards meaningful conclusions.
From the university, I was offered critical insights that challenged me to think deeply about my work by Oriol Colomés and Sander van Nederveen. The feedback from my academic supervisors encouraged me to critically evaluate my research. Through this, the process of reflection and adaptation was extended to every facet of my work, allowing me to integrate it into a comprehensive approach for my research.
The technical and soft skills gained by my company supervisors Matteo Capaldo, Marianna Rondon, and Zaid Allybokus at TotalEnergies have been equally valuable. They introduced me to new dimensions of modeling and computing, and taught me how to effectively communicate the essence of the project. Their mentorship was important in translating complex technical concepts into clear, impactful messages.
The support from the wind department at TotalEnergies went beyond mere academic assistance; it provided a foundation for my professional growth. The experience of performing my research in the presence of industry experts offered me a glimpse into the workings of the field and inspired me to embark on my own career path with confidence and enthusiasm. Special thanks to Christina Khalil and Cynthia Tayeh, who were always willing to advise and assist me in this project with their profound academic knowledge.
My peers and family have also provided unwavering support, for which I am deeply thankful.
This thesis is a product of the collective effort and dedication of everyone involved. It is my hope that the work presented will contribute to the field of renewable energy and aid in the development of efficient and sustainable offshore wind energy.

Niels Roeders
Paris, July 2024

Abstract

Offshore wind farms, critical for sustainable energy production, face the challenge of optimization among many parameters influencing the objectives in conflicting ways. In response, this research introduces the novel Integrative Maximized Aggregated Preference Wind Farm Optimization (IMAP-WFO) framework—a comprehensive tool designed to enhance the flexibility, accuracy, and uncertainty quantification of offshore wind farm design and operation.

Existing methods often fall short due to limitations in adaptability and precision, especially when modeling complex multi-physical behaviors under uncertain conditions. IMAP-WFO represents a fundamental change by combining advanced statistical techniques and simulation methods.

At its core are parametric design performance functions, capturing critical aspects of wind farm behavior, including energy production, material usage, and structural fatigue. These functions rely on Kriging meta-models, known for their accurate predictions of unknown values. To address inherent uncertainty, Monte Carlo simulations provide a probabilistic assessment of outcomes. IMAP-WFO's true innovation lies in translating technical functions into socio-economic objectives. These include sustainability metrics, Annual Energy Production (AEP), Capital Expenditure (CAPEX), Operational Expenditure (OPEX), model uncertainty, and lifetime fatigue. Stakeholders can dynamically weigh these objectives based on their preferences, showcasing IMAP-WFO's versatility.

A validation process described in this research ensures the accuracy of design performance functions, comparing simulated results with real-world data from operational wind farms. IMAP-WFO's application is demonstrated through case studies: optimizing the Levelized Cost of Energy (LCOE) and exploring wind farm control strategies. Overall, IMAP-WFO bridges the gap between technical challenges and socio-economic goals, helping offshore wind farm design to increase in efficiency.

Contents

List of Figures

List of Tables

Glossary

Variables and symbols

A	Scale factor	[-]
A_b	cross-section	$[m^2]$
A_{rotor}	Rotor area	$[m^2]$
a, m, & k	material-specific constants	[-]
c	Fatigue ductility exponent	[-]
$C_p(\lambda, \beta)$	Power coefficient	[-]
C_T	Thrust coefficient	[-]
D	Rotor diameter	[m]
deltaF	Stress range	$[\frac{N}{m^2}]$
D_F	Lifetime fatigue damage	[-]
E_t	Electricity generation in year t	[MWh]
$f(x)$	Objective function	[-]
$factor_{lifetime}$	Lifetime factor	[-]
F_g	Top load	[kN]
$g_j(x)$ & $h_l(x)$	Constraint functions	[-]
H	Waterdepth	[m]
H_s	Significant wave height	[m]
I	Moment of inertia	$[m^4]$
I_a	Ambient turbulence	[-]
I_c	Cable current	[A]
I_t	Investment expenditures in year t	[€]
I_+	Added turbulence	[-]
k	Shape factor	[-]
$L_{\text{cable,x}}$	Cable length at point x	[m]
M	Bending moment	[kNm]
M_{found}	Foundation mass	[ton]
M_t	OPEX in year t	[€]
m_{ts}	Topside weight	[ton]
n	Economic life of the system years	[-]
$N_{\sigma,occur}$	Fatigue cycle life	[-]
$n_{\sigma,occur}$	Stress range cycle-count	[MW]
P_{gen}	Generated power	[MW]
P_{rated}	Cable rated power	[MW]
P_{trans}	Transported power	[-]
r	Autocorrelation function (or kernel)	[Ω]
R_{cable}	Cable resistance	[-]
r_{dis}	Discount rate	[°]
SA	Angle of inertenal friction	[s]
T_p	Wave period	[m]
t_{ref}	Reference thickness	[m]
t_{tt}	cross-section thickness	[kV]
V	Cable rated voltage	[m/s]
V_{WS}	Windspeed	[-]
X	Slope factor	[m]
x	Turbine spacing	[-]
x_i	Design variables	[-]
Y	Waterdepth slope factor	[-]
Z	Jacket weight factor	[-]
θ	Hyperparameters meta model	$[\frac{kg}{m^3}]$
ρ	Air density	
σ	Stress	$[\frac{N}{m^2}]$
σ_Z^2	Variance of the Gaussian process	[-]
$0.5 * \Delta\varepsilon^{\text{p}}$	Plastic strain amplitude	[-]
ε_{f}'	Fatigue ductility coefficient	[-]

Abbreviations

AEP	Annual Energy Production	[MWh]
AHV	Anchor Handling Vessel	[-]
BoP	Balance of Plant	[-]
CAPEX	Capital Expenditure	[€]
CF	Capacity Factor	[-]
COV	Cost of Valued Energy	[€]
CV	Coefficient of Variation	[-]
DALYs	years lost or disabled due to a disease or accident	[years]
FCR	Fixed Charge Rate	[-]
GA	Genetic Algorithm	[-]
HFO	Heavy Fuel Oil	[-]
HPC	High-Performance Computer	[-]
IMAP	Integrative Maximised Aggregated Preference	[-]
LCOE	Levelized Cost Of Energy	[€]
LDR	Linear Damage Rules	[-]
MCS	Monte Carlo Simulation	[-]
MODO	Multi-Objective Design Optimization	[-]
MSE	Mean Squared Error	[-]
NPV	Net Present Value	[€]
OPEX	Operational Expenditure	[€]
OSV	Offshore Support Vessel	[-]
PDF	Probability Density Function	[-]
PSO	Particle Swarm Optimization	[-]
RNA	Rotor Nacelle Assembly	[-]
ROI	Return on Investment	[-]
SODO	Single Objective Design Optimization	[-]
SD	Standard Deviation	[-]
TS	Tip Speed	[m/s]
TSR_{opt}	Optimal Tip Speed Ratio	[-]

1

Introduction

1.1. Research context

In the face of a rapidly growing global demand for renewable and sustainable energy sources, the need to increase the efficiency and competitiveness of renewable energy technologies has become more critical than ever. The transition to cleaner energy sources is not only a response to environmental concerns but also a strategic move toward energy security and economic sustainability. As such, there is an ever-growing need to develop innovative approaches. These developments should not only take place in creating new methods to harness renewable energy but also optimize production for existing methods, making it cost-effective and competitive in comparison to conventional fossil energy sources.

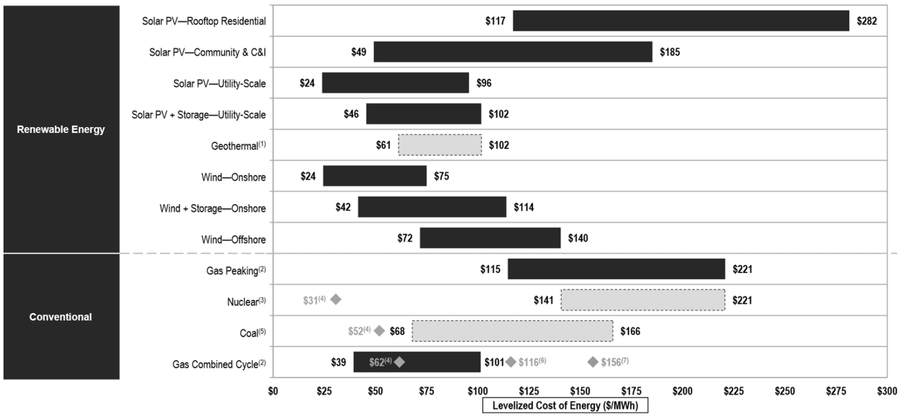

Figure 1.1: Levelized Cost Of Energy Comparison *2023 Levelized Cost Of Energy+* [1]

As can be seen in Figure 1.1, while making significant steps, the renewable energy market still faces challenges associated with the cost of energy production. To make renewable energy more accessible and economically viable, it is essential to reduce costs across the entire lifecycle of renewable energy projects. Offshore wind energy has emerged as a particularly promising solution for meeting renewable energy targets due to the vast potential of wind resources over open waters Lynn [28]. Offshore wind farms offer several advantages such as stronger and more consistent wind speeds, mitigated visual impact, and the ability to harness wind resources near densely populated coastal regions. However, the offshore environment poses unique challenges, including harsh weather conditions, logistical challenges in construction and maintenance, and economic viability [28].

1.2. Research problem

The growing demand for offshore wind energy as a sustainable power source is still being limited by the high levelized cost of energy (LCOE) when compared to traditional fossil energy Voormolen, Junginger, and Van Sark [45]. One of the challenges lies in the effective optimization of offshore wind farm designs and the control of the farm. A standard approach for optimization is to optimize a single objective such as cost or production Rodrigues, Bauer, and Bosman [34]. A promising procedure for addressing this challenge is through the application of Integrative Maximised Aggregated Preference (IMAP) optimization methods, which allows for an optimized design based on multiple objectives while being guided by defined operator strategies.

Despite various studies exploring offshore wind farm optimization, the specific application of a probabilistic IMAP procedure defined by multi-objective design optimization (MODO) and operator strategies, remains largely unexplored. The existing gap in research thus relates to the absence of studies that address the optimization of offshore wind farm layouts through this IMAP approach, considering MODO operator strategies. Additionally, the incorporation of probabilistic design performance functions, accounting for uncertainties, will be a focal point of investigation.

1.3. Research objectives

The global goal of this research is to reduce the LCOE associated with offshore wind power generation by implementing a robust optimization framework for wind farm design and control. Specifically, the focus is on linking the specific wind farm characteristics to align with client strategies, ultimately enhancing operational efficiency and maximizing energy production, based on the determined strategies. Through this tailored optimization, the research seeks to contribute an innovative solution that steers offshore wind energy towards increased cost-competitiveness in comparison to conventional fossil energy sources.

1.4. Research scope

This research will explore the adaptation of Integrative Maximised Aggregated Preference (IMAP) optimization, focusing on the strategic conflicting objectives of a single client in contrast to traditional IMAP approaches where preferences from multiple stakeholders are considered Heukelum et al. [18]. A comparative case study will be integral to validating the effectiveness and proof of concept of this client-centric IMAP optimization.

The research will focus on bottom-fixed monopile three-bladed upwind wind turbines. An examination of these assets through a system behavior framework, encompassing fatigue, Annual Energy Production (AEP), material usage, and vessel usage, will clarify the performance characteristics on which the strategies can be employed.

A key facet of this research involves probabilistic design, introducing variability into the variables associated with the design of the offshore wind farm. These variables will be modeled with probabilistic spreads through which a Monte Carlo Simulation (MCS) can give the final uncertainties in the model.

For verification, there will be a comparative case study, drawing comparisons between the outcomes of the probabilistic strategy-based IMAP optimization and traditional optimization outcomes. This comparative approach will serve as a verification tool, offering proof of concept of the proposed IMAP optimization strategy.

1.5. Resarch questions

Answering the main research question forms the main goal of the research. This question can be answered by first finding the answers to the supporting questions.

1.5.1. Main research question

How is the LCOE influenced by employing a probabilistic multi-objective strategy based Integrative Maximised Aggregated Preference (IMAP) optimization approach in the design of offshore wind farms?

1.5.2. Supporting research questions

- What are the key design variables optimizable in offshore wind farms, and how do these variables impact the cost and production characteristics of such wind farms? How can these impacts be quantitatively expressed?

1. What are the fatigue characteristics of the investigated structures based on optimized variables, and how can these characteristics be modeled in a simplified analytical expression?
2. What materials are used in offshore wind farms, and how does their dependency on optimized variables manifest? How can this dependency be expressed?
3. What are the environmental impacts of a wind farm design based on optimized variables?
4. In what manner can the production of wind turbines be expressed based on the optimized variables?
5. What uncertainties exist in offshore wind farms based on optimized variables, and what methods can be employed to quantify these uncertainties in the final design?

- What methods can be employed to capture and quantify the strategy of the operator in the layout design of offshore wind farms? How can this strategy be integrated into the characteristics of an offshore wind farm to guide decision-making?
- In what way can the developed model be effectively verified? How can it be compared to an executed project to provide evidence of the reduction in LCOE achievable through the proposed probabilistic strategy-based IMAP optimization approach in wind farm design?

From the introduction here in chapter 1, the main investigated in this research already becomes apparent. In chapter 2, the theoretical background necessary for this specific research is given and explained. Onwards, in chapter 3, the existing state of the art is identified for the most significant categories in wind farm optimization. From this, the research gap that will be filled through this research is identified. In chapter 4, the methodology to fill the research gap and answer the research question is giving. This is done through the creation of the IMAP-WFO model which is composed of design performance- objective-, and preference functions. In chapter 5, the design performance functions are verified towards existing wind farms and in chapter 6 two case studies are performed with the created model. The goal of the first case study is to show the models capability to compete with existing optimization models by minimizing the LCOE for an existing wind farm. The second case study shows the true added value of the proposed model by optimizing the control of a wind farm based on energy price and fatigue. Finally, in chapter 7, these results are interpreted, limitations are given, conclusions are drawn, the impact is given and perspective regarding follow-up studies and model improvements is supplied.

2 Theoretical Framework

In the following sections, all relevant theories for wind farm optimization are identified. The theoretical aspects behind the modeling approaches adopted for the probabilistic parametric optimization model are summarized. First, the broader model theories which are used will be explained. These are design optimization, IMAP-based optimization, probabilistic design, and the Kriging meta-model. These models are supported by different distributions, which are explained later. Finally, the LCOE, fatigue, and energy production are explained, which play an important role in wind farm design.

2.1. Design optimization

Optimization is the process of finding the most effective or favorable value or condition. Optimization processes are essential across various scientific disciplines, especially in rapidly evolving engineering applications, where there is a constant need for design improvements. The following sections explain the core components of an optimization process.

An optimization workflow manipulates specific variables that define the system (design variables) to enhance certain properties (objectives) while ensuring other properties remain within specified limits (constraints). Mathematically, an optimization problem can be expressed as follows:

$$\begin{aligned} &\text{minimize } f(x) \text{ by varying } x_i \text{ within } \underline{x}_i \leq x_i \leq \overline{x}_i \quad (i = 1, \dots, n_x) \\ &\text{subject to } g_j(x) \leq 0 \quad (j = 1, \dots, n_g) \\ &h_l(x) = 0 \quad (l = 1, \dots, n_h) \end{aligned}$$

Here, $f(x)$ is the objective function , x_i represents the design variables. and $g_j(x)$ and $h_l(x)$ are the constraint functions.

2.1.1. Design Variables

Design variables (x_i) are the parameters adjusted to improve the system's objectives. Ideally, all variables affecting the objectives should be included in the optimization process. However, including more variables increases computational time and complexity. Therefore, it is crucial to identify and include only those variables with a significant impact on the objective function.

2.1.2. Constraints

Constraints ($g_j(x)$ and $h_l(x)$) limit the optimizer's design freedom and define the feasible region within which the optimizer can explore alternative designs. Constraints can be geometrical or related to structural behavior. For example, in optimizing a wind turbine's power production by increasing blade length, constraints must prevent the blades from hitting the ground.

2.1.3. Objective Functions

Objective functions ($f(x)$) evaluate the system's performance for a given set of design variables. The objective function's value changes based on the design variables and reflects the optimization goal. For instance, increasing the number of wind turbines in a wind farm increases production but may not be optimal if the objective is cost reduction.

2.1.4. Pareto front

When dealing with two or three equally important objectives, the Pareto front can be used to find the optimum solution. By varying the different design variables through the objective functions, these objective functions will give certain outputs. By creating a graph where the axis represents the objective functions range of outputs and plotting these outputs for many variations of the design variables, we create a point cloud of possible outputs of the objectives. Based on the choice of minimization or maximization for each objective, a contour is created around the points. An example of this is shown in Figure 2.1 where the capacity factor is maximized and the LCOE is minimized.

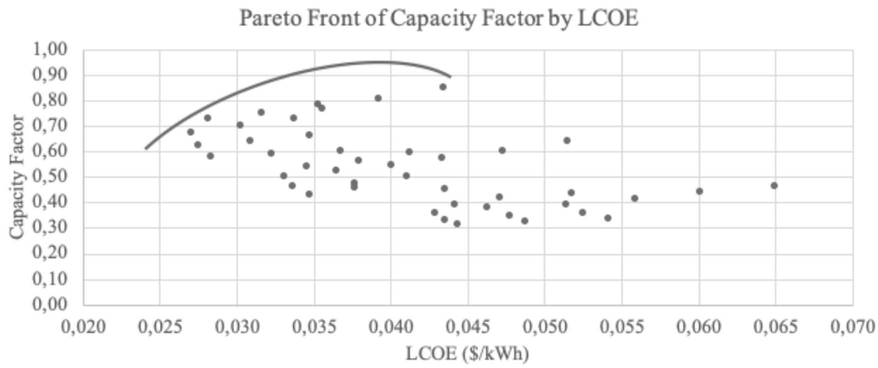

Figure 2.1: Example Pareto optimization Dykes [11]

This contour is called the Pareto front, where the optimal solutions can be found. To find the optimal solution, the Utopian point should be identified. The Utopian point is the optimal point for the optimization, in Figure 2.1 this would be LCOE= 0.02 and Capacity Factor = 1.0. The optimal solution can now be found by finding the point on or behind the Pareto front closest to the Utopian point.

2.1.5. Optimization Algorithms

Optimization algorithms guide the process of finding the optimal set of design variables. These algorithms determine the designs tested in each iteration and set the conditions for convergence.

Optimization algorithms fall into two main categories: gradient-based and gradient-free. Gradient-based methods optimize designs by evaluating if the objective function's minimum is reached based on its gradient. These methods excel when the number of variables increases, although deriving the function's gradient can become more complex. One drawback is the potential introduction of errors during gradient evaluation, particularly for complicated functions. Additionally, gradient-based methods may minimize to a local rather than a global minimum, which is influenced by the design space and initial design. A common approach to mitigate this issue is initializing the optimization from multiple points within the design space.

Gradient-free algorithms, on the other hand, focus on exploring the design space to find the minimum rather than analyzing the gradient of the initial point. Typically, gradient-free methods begin with a set of points (the population) in the design space. Based on the objective function values for these points, the optimizer assesses the design space morphology and converges to the global minimum. These methods are easier to set up compared to gradient-based methods and are suitable for optimization problems involving multiple objectives. However, they generally require more computational resources due to the need to create designs throughout the feasible space. Common gradient-free methods in offshore engineering include Genetic Algorithms (GA) and Particle Swarm Optimization (PSO). This thesis focuses on the Genetic Algorithm.

2.1.5.1 Genetic Algorithm

In the GA, the fitness of each individual in a population is evaluated using an objective function. The next generation of individuals (offspring) is produced by combining the current population (parents) based on their fitness levels. In the context of design optimization, the population comprises designs derived from different combinations of design variables. Fitness is directly related to the optimization objective, such as energy production.

The GA flowchart, as depicted in Figure 2.2, involves the following main steps:

1. **Initialization**: The process begins with a specific number of individuals forming the initial population, which is usually generated randomly unless specified otherwise.
2. **Evaluation**: Each individual in the population is assessed based on its fitness for the optimization objective. Fitness is rated through specific functions, closely linked to the objective function.
3. **Selection**: The best-performing individuals are selected to produce the next generation.
4. **Crossover and Mutation**: Selected individuals undergo crossover and mutation to create offspring, introducing variations that may yield better solutions.
5. **Iteration**: Steps 2-4 are repeated until a termination criterion is met, such as a maximum number of iterations, optimization time, or convergence of the population.

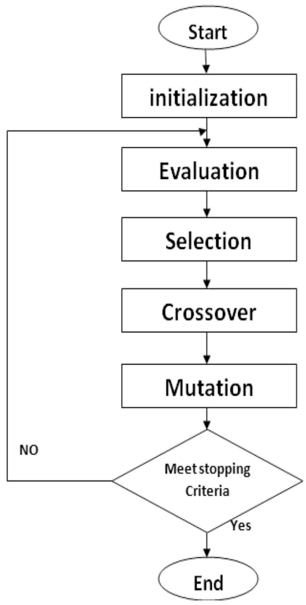

Figure 2.2: Genetic algorithm flowchart AbdulHamed, Tawfeek, and Keshk [2]

2.1.5.2 Termination Criteria

Optimization processes can be terminated based on various criteria, such as the maximum number of iterations, optimization time, or convergence indicators. For the modified IMAP GA used in this thesis, termination occurs after there have been five iterations with the same design variant with an aggregated preference score of 100. The IMAP methodology will be further explained in the next section.

2.2. IMAP optimization framework

2.2.1. Objective optimization

If an optimization model contains one objective function, this can be called a single objective design optimization (SODO) model. These models only optimize the design for their specific objective such as minimized cost or maximized profit.

If an optimization model has multiple objectives, it is deemed a multi-objective design optimization (MODO) and the model incorporates multiple objectives to find the optimal solution. The model gives the objectives certain weights based on their importance for the desired output. These MODO models are usually preferred since real design questions also contain multiple (conflicting) objectives.

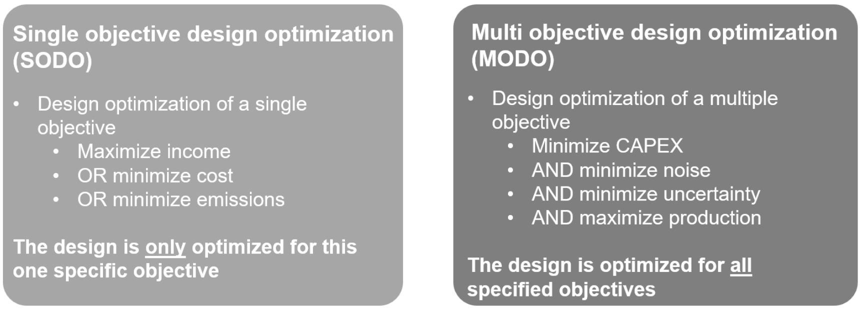

Figure 2.3: SODO and MODO

2.2.2. standard vs IMAP optimization

When using MODO for more than 3 objectives or with different objective weights, a Pareto comparison is not possible anymore. Here, the objective outcomes need to be in the same domain to make a comparison between different outputs possible, from which an optimum can be found. If the objectives' outputs are different, an optimum can not be found since the optimization model does not know how to relate the outcome of one objective in a certain unit to the outcome of a second objective in a different unit.

For this reason, standard MODO approaches use monetization of the model outcomes, to compare all outcomes in the financial domain. One of the problems with monetization is that this increases uncertainty since some outcomes are hard to monetize (e.g. noise) or some outputs have a high price fluctuation (e.g. electricity production) making the model outputs less reliable. The limitation of the Pareto front is that it can not be guaranteed if an optimal design has been reached, thus a choice has to be made between sub-optimal compromise solutions. This problem only increases with project complexity since not all design alternatives on a Pareto front can be evaluated, making it possible that an optimal solution is ignored Mueller and Ochsendorf [30].

Instead, through IMAP MODO, all model outcomes stay in their respective domain. This is made possible through the user defining their preference for certain objective outcomes using preference functions. These preference functions act as a translation function, transferring the objective outcomes in their respective domains into a certain preference score; based on the user-defined preference function for that objective. So even though all objective outcomes can stay in their respective domains, these outcomes are later translated to a preference domain through the user-defined preference functions. This is also where the outcomes are compared and an optimum is found.

Figure 2.4: Standard vs IMAP MODO

2.2.3. Preference function modelling

As discussed in the previous paragraph, the possibility to compare objective outcomes in their respective domain is made possible by the objective preference functions. These functions are defined by the user and translate their objectives and preferences into a shared domain. The user defines the objective outcome most desired with a 100 preference score and the least desired output with a 0 score. Besides this, it is up to the user to make the preference curve as simple or complex as they want.

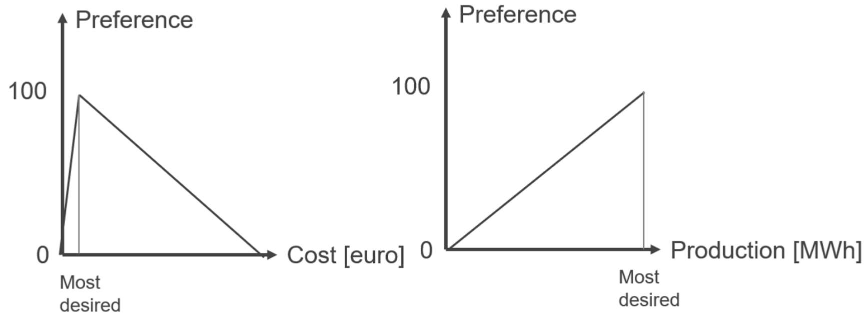

Figure 2.5: Two example preference functions for cost and production

In the above preference curves, a triangular distribution is chosen for the cost objective. A cost of 0 (x=0) is deemed unfeasible so a preference score of 0 is given for this point. A low cost (x=most desired) is given the highest preference score of 100. And then finally, a certain cost (x=X) is deemed to high and also given a preference score of 0. For the production objective, an even simpler preference curve is chosen. A production of 0 (x=0) is least desirable/ unfeasible so given a preference score of 0. A most desired production level (x= most desired) is given a preference score of 100, telling the model this is the most desired outcome for production. Please note that the x=most desired and x=X would reflect real model outcomes in the optimization model.

2.2.4. Adapted Genetic Algorithm

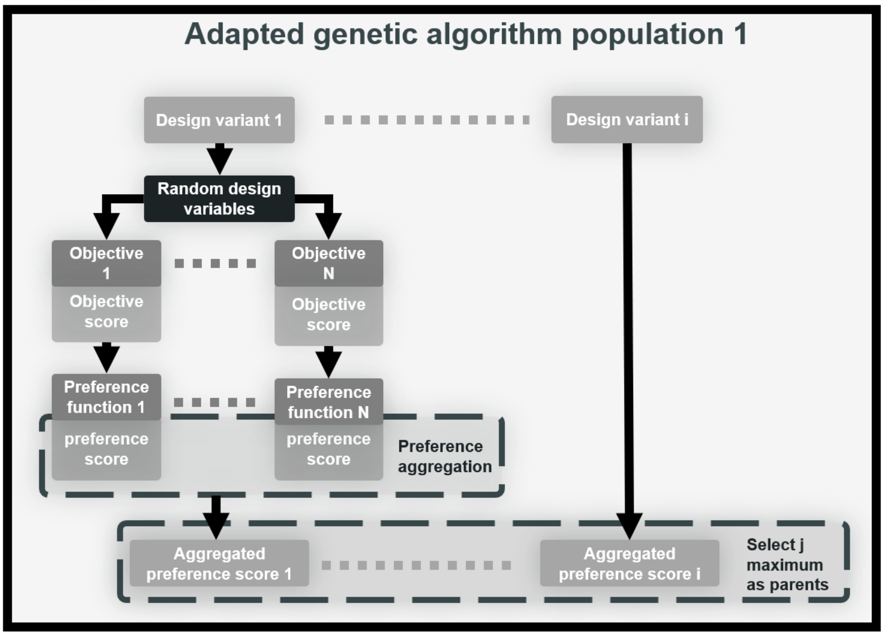

Figure 2.6: Adapted Genetic Algorithm with preference aggregation

For the IMAP methodology, a modified Genetic Algorithm is created in Heukelum et al. [18] with the novel addition of preference aggregation. The genetic algorithm works exactly the same as the one described in subsubsection 2.1.5.1 with the important difference that before evaluation, all the individual objective outcomes are coupled to their respective preference curves. After this, the population members will have a preference score for each objective separately. Based on the objective weights, these are then aggregated to give a preference score for the population members. From this, the Genetic Algorithm continues as usual, now identifying the best preference scores.

2.2.5. IMAP advantages

The most notable advantages of IMAP over a standard optimization approach are the usage of the preference domain as a shared objective domain and the possibility of more flexible optimization approaches instead of just minimization or maximization.

Firstly, the use of combining and optimizing objective outputs in the preference domain gives highly user-defined fit-for-purpose outcomes. Since the user has the possibility to steer the model outcome on the objective level, an outcome reflecting the needs of reality is made possible through this approach.

Besides this, instead of just minimizing or maximizing on an objective level; the IMAP approach gives more flexibility on specific model outcomes. It is for example possible to set an objective as a constraint by defining an objective preference function with a vertical line for a certain value towards the preference score of 100. This means that the model can only give optimal solutions where this objective has this specific model outcome (1). Next to this, it is also possible to set a certain interval for a model outcome. By defining this, a certain outcome is still most desired but lower or higher values are still possible but with lower preferences. This gives rise for the possibility to map concessions in design questions. There is a certain optimum outcome for a specific objective, and a deviation from this can be discouraged while still made possible (2). Finally, it is also possible to leave a certain objective out by defining its weight as 0. In that case, the optimization model will see this objective as irrelevant and not take the preference curve into consideration (3).

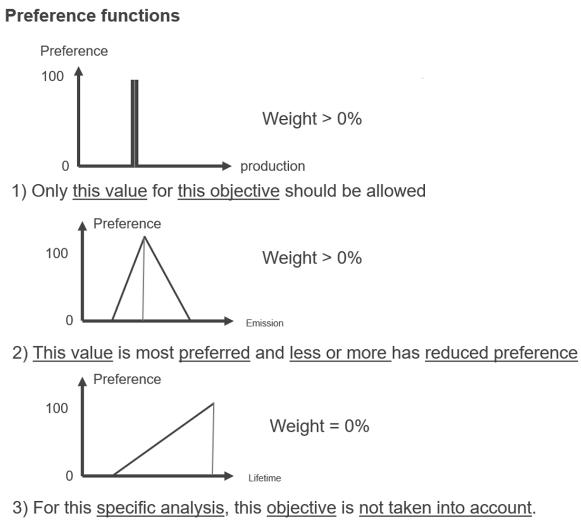

Figure 2.7: Three flexible examples for preference curves

2.3. Probabilistic design (Monte Carlo)

In a Monte Carlo simulation (MCS), the model parameters are treated as stochastic instead of fixed, deterministic, values. This approach is grounded in the principle of randomness, where the ability to generate a sequence of independent numbers from defined distributions is crucial for the model parameters Bonate [6]. By sampling these variables from their respective distributions, one can determine a model output that reflects the inherent uncertainty of the input variables.

However, the result obtained represents the uncertainty for only one iteration. To achieve a robust statistical output, the MCS must be performed with a sample size larger than one and preferably close to 10,000, denoted as N. This repetition allows for the accumulation of a comprehensive set of outcomes, which can then be used to perform a probability analysis. Through this, the output of each iteration can be plotted against its probability, creating a distribution of possible outcomes.

The true value of an MCS lies in its capacity to execute a model (N) times, thereby enabling the generation of a probabilistic model output. This output is not merely a single point estimate but a probability distribution, providing a spectrum of possible results along with their likelihoods. Such a distribution is valuable for risk assessment and decision-making processes, as it offers a visual and quantitative method to understand and communicate the uncertainty associated with the model's predictions.

2.4. Machine Learning

Surrogate models are essential tools in computational simulations, enabling efficient approximations of complex physical phenomena without the need for extensive computation. These models can be broadly classified into two categories: physics-based and data-driven models. Physics-based surrogate models, such as Reduced Basis (RB), Proper Orthogonal Decomposition (POD), and Model Order Reduction (MOR), simplify the underlying physical equations to reduce computational costs. This simplification, however, often comes at the expense of some degree of accuracy. On the other hand, data-driven surrogate models use response surface modeling to fit an approximated function directly to empirical data, eliminating the need to solve physical equations after the model has been trained. This approach generally leads to significantly faster evaluations, making data-driven models particularly advantageous in scenarios where numerous evaluations are required.

Data-driven surrogate models rely on machine learning techniques to approximate the relationship between inputs and outputs. The process typically involves splitting the available dataset into training and validation subsets, commonly using an 80-20 ratio Morozova et al. [29]. The training set is employed to fit the model, while the validation set is used to assess its performance. This train-test split is crucial for ensuring the model's ability to generalize to unseen data. Various supervised learning methods are employed in creating data-driven surrogate models, each with its own set of advantages and disadvantages. For instance, linear regression is simple and interpretable but limited to modeling linear relationships. Support Vector Machines (SVM) are powerful for high-dimensional spaces but can be computationally intensive and sensitive to the choice of kernel. Random Forests, an ensemble learning technique, are robust and handle non-linear relationships well but may require significant computational resources for large datasets. Convolutional Neural Networks (CNN), often used for image-like data, are capable of capturing complex patterns and feature hierarchies but necessitate large amounts of data and computational power for training.

One of the critical advantages of machine learning-based surrogate models is their ability to handle complex and non-linear relationships within the data. However, a significant challenge lies in acquiring a sufficiently large and high-quality dataset to train the model effectively. Moreover, selecting the appropriate machine learning technique is crucial to ensure that the model can accurately capture the underlying dynamics of the problem.

Kriging meta-modeling, a form of Gaussian Process Regression (GPR), offers several unique benefits that make it a powerful tool for surrogate modeling. Kriging is particularly well-suited for situations where data points are sparse, as it can produce reliable predictions with a relatively small dataset. This method is advantageous in high-dimensional spaces, where collecting large amounts of data can be impractical or prohibitively expensive. Additionally, Kriging's anisotropic behavior allows it to account for varying levels of smoothness in different directions of the input space, enhancing its ability to model complex phenomena accurately. Furthermore, Kriging provides not only predictions but also uncertainty estimates for those predictions, which can be invaluable in assessing the confidence of the model's outputs.

The accuracy and speed of Kriging make it an ideal choice for many engineering and scientific applications, particularly in fields where computational resources are limited or where quick, reliable approximations are necessary.

2.5. Kriging meta-modelling

In many engineering applications, numerical analyses are widely used for predicting system responses that have not been observed. However, these analyses often require significant computational resources, making them impractical for direct inclusion in optimization models that need numerous simulations. To bypass this issue, meta-modeling techniques have been devised as a surrogate to the computationally intensive original models. A meta-model serves as an approximation of the original model, which is treated as a black-box function, inaccessible to the users. It is constructed using a dataset of input values (x) and corresponding output observations (y), which are typically split into training and validation sets to ensure the model's accuracy and generalizability. The use of these training and validation points can be seen in Figure 2.8 Huchet [19].

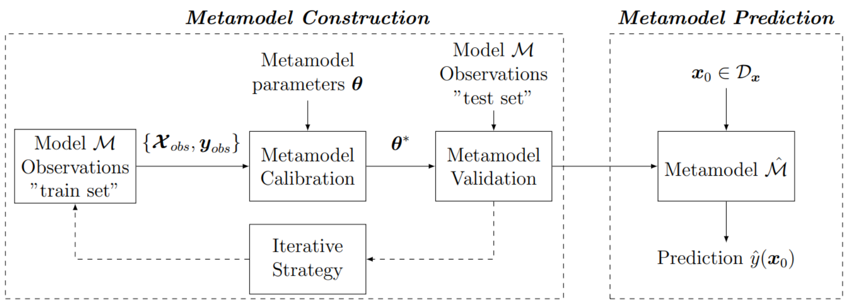

Figure 2.8: Metamodel construction and prediction [19]

One of the main benefits of kriging meta-models is the possibility of defining a variance of estimation for each prediction, known as the Kriging variance. This feature is instrumental in quantifying the uncertainty of the meta-model's responses. The Kriging prediction itself is formulated through a multivariate Gaussian distribution, defined by its mean vector and covariance matrix. The calibration of this covariance matrix is achieved through hyperparameters, as noted by Huchet [19]. The stationary Gaussian process (Z) is characterized by an autocovariance function, which can be expressed as Equation 2.1.

$$\mathrm{Cov}\left[Z_1, Z_2\right] = \sigma_Z^2 r\left(x_1 - x_2, \theta\right) \text{ for all } \left(x_1, x_2\right) \in \mathcal{D}_x \times \mathcal{D}_x \tag{2.1}$$

where,
σ_Z^2 is the variance of the Gaussian process
r the autocorrelation function (or kernel) which hyperparameters are regrouped into vector θ

The autocorrelation function is instrumental as it determines the degree of similarity between points based on their relative positions in the input space. The choice of this function and its hyperparameters significantly influences the meta-model's predictive performance. By optimizing these hyperparameters, one can tailor the kriging meta-model to accurately reflect the underlying physical phenomena it is intended to simulate.

Kriging meta-models are particularly advantageous in scenarios where the objective is to gain insights into the behavior of complex systems without incurring the high costs of full-scale simulations. They enable practitioners to optimize design parameters, and conduct uncertainty quantification with greater efficiency.

2.5.1. Covariance matrix (kernel)

Kernels play a fundamental role in the construction of kriging meta-models, serving as parametric functions that encapsulate the statistical dependencies between observations. For this application, the choice of a stationary correlation kernel is important, as it argues that the correlation between any two inputs depends solely on their relative shift, not on their absolute positions. This assumption simplifies the model and makes it more manageable. From this, the squared exponential anisotropic correlation function can be found. This is a specific type of kernel that is widely used due to its smoothness and mathematical properties. The advantage is that this function can capture different physical behaviors for different dimensions, which is important for the needed applications. It can be expressed as Equation 2.2 [19].

$$r(x_1, x_2, \theta) = \exp\left(-\frac{1}{2}\sum_{i=1}^{n}\left(\frac{x_{1,i} - x_{2,i}}{\theta_i}\right)^2\right) \tag{2.2}$$

This function decreases exponentially as the distance between the input points x_1 and x_2 increases, with the rate of decrease controlled by the hyperparameters θ. The hyperparameters θ_i are crucial as they determine the length scale of the correlation in each dimension of the input space, thus allowing the model to capture anisotropy (where different directions in the input space may have different levels of correlation).

Furthermore, the choice of kernel affects the smoothness of the resulting meta-model. With its infinite differentiability, the squared exponential kernel ensures that the meta-model will also exhibit a high degree of smoothness. This is beneficial when the true system's behavior is similarly smooth but less appropriate for functions with discontinuities or abrupt changes [19]. However, the meta-model accuracy is not extremely sensitive to kernel choice and more sensitive to hyperparameter calibration Powell [32].

2.5.2. Hyperparameters

In the context of Kriging meta-models, the calibration process is crucial to ensure that the model accurately reflects the underlying physical behavior it is intended to simulate. Before utilizing a kriging meta-model, it is important to calibrate it to fit the model to the specific characteristics of the data at hand. This process involves several key steps:

- **Autocorrelation Model Specification**: Initially, the user must determine the type of autocorrelation function to be used. This decision is typically made by expert judgment or insights gained from preliminary studies. The autocorrelation function defines how data points relate to each other based on their spatial or temporal distance.
- **Hyperparameter Estimation**: Once the autocorrelation model is specified, the next step is to estimate the hyperparameters. These are parameters that govern the behavior of the autocorrelation function and, by extension, the kriging model itself. The estimation is performed using the available dataset. This first estimation will form the starting point for finding the actual hyperparameters.
- **Training and Validation Set Creation**: A subset of the full dataset is randomly selected to form the training and validation sets. The proportion of data allocated to training is predetermined by a set training percentage. The training set is used to build the model, while the validation set is reserved for testing its predictive accuracy.
- **Meta-Model Setup and Calibration**: The meta-model is configured based on the training dataset. Calibration is then achieved by comparing the meta-model's predictions against the observed values in the validation dataset. This comparison is quantified using the Mean Squared Error (MSE), which measures the average of the squares of the errors between predicted and observed values.
- **Hyperparameter Selection Function**: A function is defined to select the hyperparameters by returning the MSE as its output. This function encapsulates the calibration process and serves as the objective function for the subsequent optimization step.
- **Minimization Algorithm Execution**: The hyperparameter selection function is executed within a minimization algorithm. The goal of this algorithm is to find the set of hyperparameters that result in the minimal MSE. The hyperparameters that achieve this are deemed the most accurate and are denoted by θ
- **Final Meta-Model Creation**: With the optimal hyperparameters θ identified, the final meta-model is constructed for the complete dataset. This model is expected to have reliable predictive capabilities due to the calibration process it has undergone.

By following these steps, the kriging meta-model is fine-tuned to provide reliable predictions, which is essential for its application. However, the success of the calibration process hinges on the quality of the data and the appropriateness of the chosen autocorrelation model and hyperparameters. It's a delicate balance between model complexity and predictive performance, aiming to achieve a model that is both accurate and generalize-able.

2.6. Distributions

For the MCS, stochastic variables need to be defined as distributions to sample from. In this section, the samples used in this thesis are discussed and motivated.

2.6.1. Weibull

The Weibull probability distribution is a widely used statistical calculation of wind resources, it represents the distribution of wind speed at a given site Wais [46]. The Probability Density Function (PDF), composed of the shape and scale parameters (k and A respectively), is utilized both to sample the wind-speed for the MCS and for the power production. The equation for the PDF is given in Equation 2.3 [46].

$$p(v) = \left(\frac{k}{A}\right)\left(\frac{v}{A}\right)^{k-1} e^{-\left(\frac{v}{A}\right)^{k}} \tag{2.3}$$

where:
v is the wind speed [m/s]
k is the shape factor [-]
A is the scale factor [-]

2.6.2. beta-PERT

In project planning, it is common practice to produce multiple estimates for project activity completion time. These completion times can be grouped into a minimum, most likely, and maximum completion duration, which tries to take the risk of unanticipated factors into account. With these three different completion times, random durations can be introduced to each activity by fitting a beta-PERT distribution to the completion times. Beta-PERT distribution is a commonly used method for modeling expert data when a minimum, most likely, and maximum value are known and a sample needs to be drawn from this. This creates one simulation instance of the planning where the activities are given a random duration based on their minimum, most likely, and maximum completion time to account for unanticipated factors. The equation for the beta-PERT distribution can be found in Equation 2.4 [23].

$$\begin{aligned}
p(x \mid a, b, \alpha, \beta) &= \begin{cases} 0, \text{ for } x < a, \\ \frac{(x-a)^{\alpha-1}(b-x)^{\beta-1}}{B(\alpha,\beta)(b-a)^{\alpha+\beta+1}}, \text{ for } a \leq x \leq b, \\ 0, \text{ for } x > b, \end{cases} \\
\alpha &= 1 + 4\frac{c-a}{b-a}, \\
\beta &= 1 + 4\frac{b-c}{b-a},
\end{aligned} \tag{2.4}$$

where:
a corresponds to the minimum value, b to the maximum value, and c to the most-likely value.

2.6.3. JONSWAP

The JONSWAP spectrum is an empirical relationship that defines the distribution of energy with frequency within the ocean. The spectrum is in essence an adaptation of the Pierson-Moskowitz spectrum with the distinction that the wave spectrum is never fully developed and can develop further due to non-linear wave-wave interactions for a long time. Therefore in the JONSWAP spectrum, waves continue to grow with distance as specified by the α term, and the peak in the spectrum is more pronounced, as specified by the γ term. The JONSWAP spectrum equation can be found in Equation 2.5 Carter [8].

$$E(f) = \alpha g^2 (2\pi)^{-4} f^{-5} \exp\left[-\frac{5}{4}\left(\frac{f}{f_m}\right)^{-4}\right] \cdot \gamma^q \tag{2.5}$$

where

$$q = \exp\left[-(f - f_m)^2 / 2\sigma^2 {f_m}^2\right]$$

and

$$\sigma = \begin{cases} 0.07 & f < f_m \\ 0.09 & f \geq f_m \end{cases}.$$

For the mean JONSWAP spectrum

$$\gamma = 3.3.$$

Since the JONSWAP spectrum represents the distribution of wave energy, it is used to sample the wave period and significant wave height from the energy distribution.

2.7. Levelized Cost Of Energy (LCOE)

The LCOE is often used to describe the economic performance of a wind farm. The LCOE is the total amount of power over the lifetime of an energy source, divided by the life cycle costs over the lifetime of the same energy source, as described by Equation 2.6 [12] or Equation 2.7 [11].

$$\mathrm{LCOE} = \frac{\sum_{t=1}^{n} \frac{I_t + M_t + F_t}{(1+r_{dis})^t}}{\sum_{t=1}^{n} \frac{E_t}{(1+r_{dis})^t}} \tag{2.6}$$

$$LCOE = (FCR * CAPEX + OPEX)/AEP \tag{2.7}$$

Where:
I_t : Investment expenditures in year t
M_t : Operation and maintenance expenditures in year t
E_t : Electricity generation in year t
r_{dis} : Discount rate
n : Economic life of the system
FCR: Fixed charge rate, the percentage of the cost per year to cover the minimal annual revenue requirements
$CAPEX$: The capital expenditures
$OPEX$: the operational expenditures
AEP: The annual energy production

2.8. Fatigue (Miners Rule)

Metals exhibit damage by fatigue when subjected to repeated cyclic loads. Fatigue is characterized by the principle that a single load does not have the stress magnitude to cause failure, but that this happens over a large number of cycles. The failure mechanism of fatigue is the creation of cracks in a material. The growth of these cracks increases until the critical crack size of the material under operation load is reached, leading to rupture. Since these cracks form under a load that is usually lower than the tensile strength of the material, this crack propagation can take a long time. This in turn gives the structure a long fatigue lifetime Bhat and Patibandl [4]. Wind turbines can be classified as ”fatigue critical machines” because of the unique load spectrum. For this reason, the design of many of their components is dictated by fatigue considerations Sutherland [40]. Fatigue is caused by a series of stress-strain cycles in a time series. The recognized standard for fatigue analysis of wind turbines is the Palmren-Miner linear damage rule (Miner rule), as can be seen in Equation 2.8.

$$\sum_{i}^{M} \frac{n_i}{N_i} = \frac{n_1}{N_1} + \frac{n_2}{N_2} + \frac{n_3}{N_3} + \dots + \frac{n_M}{N_M} = \mathcal{D} \tag{2.8}$$

Where the total fatigue damage $\mathcal{D}$ of a structure is calculated by n_i stress cycles at stress level σ_i for all stress levels i divided by N_i which denotes the number of cycles to failure at the same stress σ_i. Miner's rule assumes structural failure occurs when the damage equals one. Usually, the fatigue cycles are measured over a fixed timeframe. Thus, $\mathcal{D}$ is expressed as the damage rate $\Delta\mathcal{D}_t$ When this damage rate is representative of the average damage rate over the service lifetime, the service lifetime can be calculated as in Equation 2.9

$$T = \frac{1}{\Delta\mathcal{D}_t} \tag{2.9}$$

The number of cycles to failure N_i is typically described by an S-N curve and is material-specific. These curves are experimentally determined, where a specimen fails under N loads at a specific σ. The limitations of these curves are that they only provide fatigue life without giving an indication about the cycles that cause crack initiation and propagation Bhat and Patibandl [4].

There is a multitude of theories that look into the characteristics of fatigue curves. In this research, the focus will be placed on the Linear Damage Rules (LDR). Even though this theory leads to an unsatisfactory life prediction due to the load level independence, load sequence independence, and lack of load-interaction accountability Bhat and Patibandl [4]; it is easily computable, comparable between different loading scenarios and forms the industry standard. Since the fatigue damage will need to be calculated for an optimization problem, comparability, and low computational intensity are vital.

In LDR, a distinction can be made between the high-cycle elastic deformation regime (N< 10^4) and the low-cycle plastic deformation regime (N> 10^4). The high cycle regime is introduced by Basquin and can be seen in Equation 2.10

$$\sigma_{\mathrm{a}} = \frac{\Delta\sigma}{2} = \sigma_{\mathrm{f}}' \left(2\ \mathrm{N_f}\right)^{\mathrm{b}} \tag{2.10}$$

Where,
σ_{f}' is the fatigue strength coefficient
($\mathrm{N_f}$) is the number of full cycles leading to failure
b is the fatigue strength component.

The low cycle regime was introduced by Coffin and Manson and can be seen in Equation 2.11

$$\frac{\Delta\varepsilon^{\mathrm{p}}}{2} = \varepsilon_{\mathrm{f}}' \left(2\ \mathrm{N_f}\right)^{\mathrm{c}} \tag{2.11}$$

Where,
$\frac{\Delta\varepsilon^{\mathrm{p}}}{2}$ is the plastic strain amplitude
$\varepsilon_{\mathrm{f}}'$ is the fatigue ductility coefficient
c is the fatigue ductility exponent.

2.9. Energy production

A wind turbine's power curve relates the speed of the wind flow intercepted by the wind turbine rotor to its electrical output. For this reason, a power curve is often used to estimate the aggregated power production of a wind farm. Because of this, the accuracy of power curves is a critical issue since the risk involved in building and operating a wind farm is directly dependent on these Saint-Drenan et al. [35].

A power curve is composed of 4 distinct operating regions, as can be seen in Figure 2.9. At low wind speeds, the torque imposed by the wind on the blades is insufficient to rotate the turbine, which happens in region 1. Region 1 ends when the wind has picked up to the speed from which the turbine starts to rotate and generate electricity. The wind speed where this starts is called the cut-in speed. In region 2, the power production increases with the cube of the wind speed before reaching the threshold of rated wind speed. In region 2, the wind turbine operates with optimal efficiency. Above the rated wind speed, region 3 starts. Here, the turbine will keep the output power at the rated power through pitch control by adjusting the blade-pitch angle to keep the generated power stable. In region 3, the highest forces are exerted on the wind turbine and if the wind speed increases to the cut-off speed, the turbine feathers its blades and enters region 4. In region 4, there is no more power production and the wind turbine is operated in such a manner to minimize forces Saint-Drenan et al. [35].

The power in region 1 and 4 is equal to 0 and in region 3 equal to rated power. The most interesting region is 2, which can be calculated with the production equation Equation 2.12.

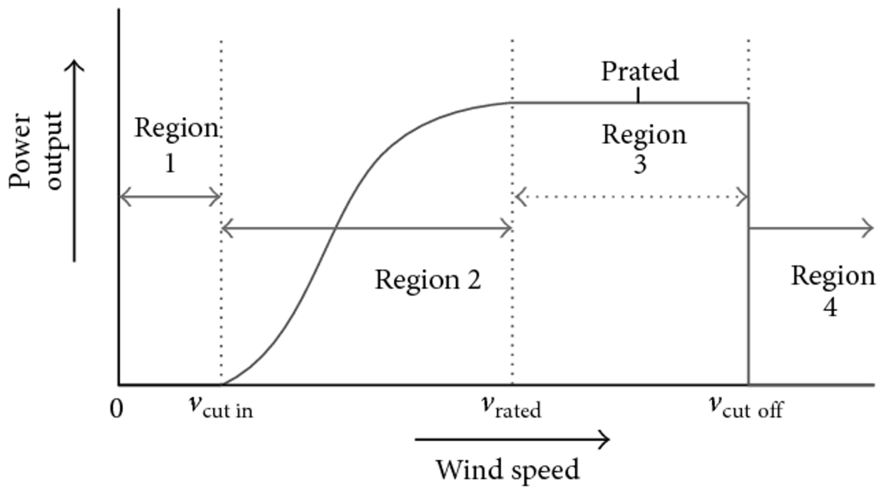

Figure 2.9: An example power curve with the distinct 4 regions.

$$P_{WT} = \frac{1}{2}\rho A_{\text{rotor}} V_{WS}^3 C_p(\lambda, \beta) \tag{2.12}$$

where,
ρ is air density [kg/m^3]
A_{rotor} is the rotor area [m^2]
V_{WS} is the wind speed [m/s]
$C_p(\lambda, \beta)$ is the power coefficient dependent on the tip-speed ratio and the blade angle [-]

3

Literature Review

In the literature review, the current state-of-the-art is identified regarding the topic of offshore wind farm optimization. Within this state-of-the-art, the main research gap is identified that this thesis will fill.

there has been a significant amount of research performed towards wind farm optimization. From simple single design variable single objective optimization in Kusiak and Song [21] to 29 design variables and four objectives in Heukelum et al. [18]. In recent years, the increase of implementing multi-objective optimization is growing, where besides production more innovative objectives can also be taken into account such as in Dykes [11].
There have been frameworks set up for wind farm layout optimization, such as in Reddy [33] that use analytical wake models and parametric cost models. Even though these models can give quick valuable designs, the analytical models show shortcomings when compared to their numerical counterparts.
Multiple key topics regarding offshore wind farm optimization are investigated wherein for each topic the state-of-the-art is identified. In the end, based on the research already performed, the research gap is identified that this research focusses on.

3.1. Design variables

The first step for starting an optimization process is defining the design variables. These are the parameters that are optimizable by the optimization algorithm. It is preferred to define these design variables, and the calculations that they are used, in parametrically. Because of this, the optimization algorithm can find solutions that are otherwise not identified if these variables are discrete. However, in some cases, these design variables are discrete since they represent existing choices (such as existing diameters or existing cables), and in other cases, these variables can be binary where 1 means the design variable occurs and 0 it does not occur.

For wind farm design, the most common design variables are geometrically related since they represent a structural design question. Even though design variables can differ, the most prevalent for wind farm design are the turbine locations. This design variable can be seen as the bare minimum requirement to perform a layout optimization. The wind turbines create aerodynamic wakes that can influence the other turbines. The turbine location is an important aspect in this matter since the wake effect is more significant if turbines are placed close together. An interesting variation on using just the turbine location can be found in Wang, Tan, and Gu [47]. Here the individual wind turbine control is included with the turbine locations.

Besides turbine locations, more complex design variables can be chosen. Rodrigues, Bauer, and Bosman [34] focus on the optimal wind farm layout, taking into account the electrical collection and delivery infrastructure. Besides the turbine locations, the turbine model, amount of substations, array cable-rated power and voltage, and export cable-rated power and voltage are included as design variables. These new design variables represent existing design choices such as the cable choice and are therefore discrete. This optimization portrays a full design synthesis in a better manner when compared to the single design variables.

Reddy [33] has proposed a wind farm optimization framework in which the placement of the turbines, rotor diameter, and tower height are taken as design variables. This is an interesting approach since the placement of the turbines and the tower height can both bedependent on the rotor diameter. The placement is dependent due to wake effect, which can be seen as a soft constraint. However, the tower height needs to be equal to the rotor radius with a certain ground clearing. This height can thus be seen as a hard constraint due to safety standards.

Faraggiana et al. [13] defines the different design parameters for a floating spar support structure as the design variables. This research focuses on the design of a single support structure instead of a whole wind farm and thus goes more into detail for the structural design.

Finally, in Heukelum et al. [18], an offshore floating wind farm is optimized towards the service lifetime design. This is the most elaborate research with regard to design variables since it makes use of 29 design variables. The first 21 design variables are of a binary nature, and represent whether a certain vessel performs a certain task. The next four design variables have a discrete nature and represent which vessel performs one specific task. The next three design variables are also discrete and represent certain anchor design choices. The last four design variables are continuous and represent different dimensions of the designed anchor. This gives an example of how an optimization framework can work with different types of design variables and it represents the most comprehensive example in this field in literature to the knowledge of the author. In Table 3.1 the discussed references for design variables in wind farm optimization are summarized.

Table 3.1: Summary of state-of-the-art references for design variables in wind farm optimization

Reference	Parametric design variable	Variable type
[21]	Turbine locations	continuous
[22]	Turbine locations	continuous
[38]	Turbine locations	continuous
[44]	Turbine locations	continuous
[43]	Turbine locations	continuous
[11]	Turbine locations	continuous
[47]	Turbine locations control	continuous
[33]	Turbine locations rotor diameter tower height	continuous
[34]	turbine locations turbine model amount of substations array cable-rated power and voltage, export cable rated power and voltage	continuous and discrete
[18]	vessel tasks anchor design choices anchor dimensions	discrete, binary and continuous

3.2. Objectives

The objective function translates the goal of the optimization model through the design variables into an optimizable output. This output and its unit thus represent the desired scale for the optimization problem. There can either be one, or multiple objectives to optimize. However, in the case of multiple objectives, these need to be on the same scale to make comparisons for analytical optimization. However, it is possible to derive a near-optimum using a Pareto front graphically. In this case, two different scales can be implemented as the x, y, and sometimes z-axis.

Usually, a production objective is used for wind farm optimization where the production is maximized. This production objective can either be expressed in energy production units such as MWh (Reddy [33] and Wang, Tan, and Gu [47]) or be expressed on a monetary scale by connecting it to other monetary key performance indicators such as CAPEX and OPEX González et al. [15]. Instead of production, Faraggiana et al. [13] minimizes the structural cost since it is a single design variable problem.

Besides only optimizing for production, it is often chosen to include an extra objective to represent other wind farm characteristics. Both Kwong et al. [22] as Sorkhabi et al. [38] also include noise as an objective besides energy production. Apart from maximizing the production, Kusiak and Song [21] also minimize the amount of constraint violations. This is an interesting approach since the constraint is thus not taken as rigid but as flexible. Veeramachaneni et al. [44] minimizes the cost of the wind farm besides the maximization of production. An interesting variation on this is presented in Rodrigues, Bauer, and Bosman [34]. Here, the total delivered energy dependent on the energy losses due to the energy collection and export system is optimized whereas costs are minimized. Besides, to look beyond the standard production quantifiers, Dykes [11] looks at the cost of valued energy and the capacity factor.

Tran et al. [43] goes one objective further and includes both the collection system length and the convex hull area of the wind farm with the energy production. However, these methods with two or three objectives do not employ the unification of the optimization scale. The objectives stay in their individual domain. These are thus mainly graphically solvable with a Pareto front or analytically with a Pareto-based Evolutionary Algorithm [34].

Unlike the other identified research, Heukelum et al. [18] has four objectives that are unified in the preference domain. These objectives are project duration, installation cost, fleet utilization, and CO_2 emission. By using the preference domain, it is possible to compare and optimize objectives with different individual scales without having to monetize them which increases uncertainty. For this reason, this is the state-of-the-art for multi-objective optimization where the objectives have different individual scales but are united in the preference domain. In Table 3.2 the discussed references for objectives in wind farm optimization are summarized.

Table 3.2: Summary of state-of-the-art references for objectives in wind farm optimization

Reference	Objective	Objective scale
[33]	AEP	Energy
[47]	AEP	Energy
[15]	NPV	Monetary
[13]	Structural cost	Monetary
[22]	AEP Noise level	GWh and dB
[38]	AEP Noise level	GWh and dB
[21]	AEP Constraint violation	GWh and [-]
[44]	AEP Cost	GWh and Monetary
[34]	delivered energy Cost	GWh and Monetary
[11]	COV CF	Monetary and [-]
[43]	AEP Collection system length Wind farm area	Monetary, Km and Km^2
[18]	project duration installation cost fleet utilisation CO_2 emission	Preference

3.3. Optimization method

When the design variables and the objectives are defined, there are multiple ways to find the design variables that give the optimum according to the objective functions. There is single-objective optimization, graphical multi-objective optimization through a Pareto front, analytical multi-objective optimization through a Pareto front-inspired Genetic Algorithm, and analytical multi-objective optimization through a preference theory-based Genetic Algorithm.

In Wang, Tan, and Gu [47], only the energy objective is maximized. This is achieved by using a Genetic Algorithm that takes the wind turbines' positions and axial induction as input arguments. Reddy [33] uses a similar approach, but instead of using just one algorithm to find the optimal solution, it uses three in its proposed hybrid optimizer. The reasoning behind this is that no single algorithm is superior to another for an entire problem set. Faraggiana et al. [13] use a Genetic Algorithm that is coupled with a Kriging surrogate model that creates new individuals in the populations based on numerical model simulations. This increases the efficiency of the GA since the population is not randomly selected but partly determined by the surrogate.

Instead of single objective optimization, Dykes [11] has multi-objective optimization. In this research, the optimal solutions are found on the graphical Pareto distribution. On the Pareto front, a selection of the optimal solution can be made. Rodrigues, Bauer, and Bosman [34] also employ a MODO optimization. However, instead of using a graphical Pareto front, here an analytical Pareto-inspired evolutionary algorithm is used. The same is the case for González et al. [15]

Finally, Heukelum et al. [18] use a different approach to find the optimal solution from its 29 design variables and four objective functions. This optimization method couples user-defined preference functions to the individual objective outputs. These preference scores are combined with a Genetic Algorithm which then finds the optimal solution based on the user-defined preferences and weights. This methodology prevents being limited to a single objective design and/ or an a-posteriori evaluation of design alternatives [5]. For this reason, the preference-inspired Genetic Algorithm (IMAP) is considered state-of-the-art. In Table 3.3 the discussed references for optimization methods in wind farm optimization are summarized.

Table 3.3: Summary of state-of-the-art references for optimization methods in wind farm optimization

Reference	Optimization method	SODO/MODO
[47]	GA	SODO
[33]	Hybrid GA	SODO
[13]	Surrogate GA	SODO
[11]	Pareto front	MODO
[34]	Pareto inspired GA	MODO
[15]	Pareto inspired GA	MODO
[18]	Preference inspired GA	MODO

3.4. Model analysis

In order to correctly predict the physical/ economic behavior of the wind turbines in the wind farm, models are necessary. These models predict the production, occurring forces, fatigue, and economic drivers. The most simple version of this can be found in Wang, Tan, and Gu [47], where only an analytic wake model is included in the model. An improvement can already be found in Rodrigues, Bauer, and Bosman [34] and Reddy [33] where the models include both an analytical wake model and economic functions and assumptions.

However, for accurate optimization results, these models need to be of the highest fidelity possible within an optimization framework. However, since these high-fidelity numerical models are usually computationally expensive, they can not be directly adapted into the optimization model. This is where a surrogate model comes into play that gives the outputs of a numerical model. This has been done in Heukelum et al. [18]. Here the outputs of the numerical model openFAST are known for discrete points. However, for even more precise results, a meta-model based on the surrogate outputs can be implemented. This model then statistically predicts the surrogate output, making the surrogate continuous. This has been done in Faraggiana et al. [13] for an in-house numerical tool calculating the hydrostatic and dynamic properties of a spar structure. This Kriging meta-modeling is considered state-of-the-art for implementing numerical models into optimization frameworks. In Table 3.4 the discussed references for modeling methods in wind farm optimization are summarized.

Table 3.4: Summary of state-of-the-art references for modelling methods in wind farm optimization

Reference	Model type	Model output
[47]	Wake model	Energy production
[34]	Wake model Economic functions	Energy production Economic drivers
[33]	Wake model Economic functions	Energy production Economic drivers
[18]	Surrogate	Forces
[13]	Kriging surrogate	Forces

3.5. Probabilistic

Since quantifying uncertainty usually involves the simulation of probabilistic distributions N times through a Monte Carlo distribution, there are not a lot of studies implementing this methodology in optimization. But, when parametrically modeling offshore wind farms with the implementation of Kriging meta-models, there is a considerable amount of uncertainty that comes into play. This problem was already identified in Li et al. [27] for optimized maintenance frameworks for offshore wind farms. This research also identifies the lack of other research on this topic. However, a large shortcoming is that in this study the estimation of uncertainty falls outside the scope.

3.6. research gap

In the current literature on optimizing offshore wind farms, some clear research gaps can be identified.

- There is no flexible optimization framework where the user himself can choose the output deemed relevant by turning objectives on and off to create different scenarios and can create model constraints through objective preferences.
- There has been some implementation of Kriging meta-modeling and MCS in wind farm optimization, but these two have not been coupled before to quantify optimization model uncertainty.
- There are no cases of predicted fatigue damage and energy production through Kriging meta-modeling in offshore wind farm optimization.
- There is no holistic optimization approach taking a multitude of wind farm socio-technical characteristics such as production, AEP, CAPEX, OPEX, lifetime fatigue, etc. simultaneously into account.

Considering this research gap, this research will investigate how the LCOE is influenced by employing a probabilistic multi-objective strategy-based IMAP optimization approach in the design and control of offshore wind farms.

4 Methodology

In order to answer the research question, an IMAP Wind Farm Optimization (IMAP-WFO) framework is created. This chapter will explain how the design performance functions reflect the technical behavior of the wind farms based on the design variables. It will also be motivated in what manner the uncertainty is quantified for each of these design performance functions. Besides this, it will be described how these design performance functions are combined into the objective functions. Here, guided by the preference functions, an optimal output will be found through the IMAP GA.

4.1. IMAP optimization

The goal of the IMAP optimization framework is to be able to find the technical and socio-technical performance of a parametrically created wind farm. Based on the boundary conditions such as the plot size, water depth, and environmental conditions, the wind farm is designed and technically evaluated through the design performance functions (fatigue, energy production, material use, and vessel use). In these design performance functions, the design variables (rotor diameter, turbine spacing, and vessel usage) are varied to create a multitude of design variants. These design variants are then evaluated based on the objective functions (sustainability, AEP, CAPEX, OPEX, lifetime fatigue damage, and model uncertainty), and guided by the preference functions, an optimal design variant is found. For this optimal design variant, the LCOE and NPV are calculated. This gives the optimal LCOE and NPV based on the given boundary conditions and defined preferences on the objectives.

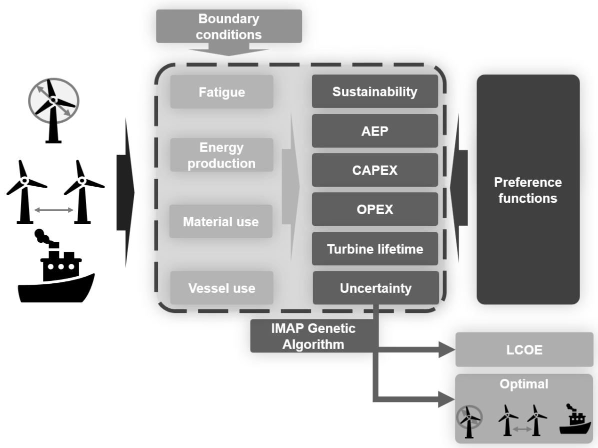

Figure 4.1: The proposed IMAP optimization model

4.2. Parametric energy production

To predict energy production, a parametric wind farm needs to be modeled and placed under certain environmental conditions. This is done through the PyWake framework Pedersen et al. [31] . A probabilistic power and thrust curve are parametrically calculated to simulate the individual wind turbines. Wind conditions and layout are simulated to model the wind farm site. The chosen wake model will calculate the wake interactions. Together, this will create a parametrically calculatable probabilistic energy production. the design variables for this building block are the rotor diameter and inter-turbine spacing.

4.2.1. Probabilistic power and thrust curves

As described in section 2.9, Saint-Drenan et al. [35] describes an in-depth manner to parametrically model power curves. Besides this description, a validated Python model is also provided which takes as main input the rotor diameter, cut-in and cut-out speed, and the rated power (calculated as in section 2.9). Besides this, it also takes environmental conditions such as turbulence intensity, wind shear, wind veer, and air density into account. From this model, the power coefficient, optimal tip speed ratio (TSR_{opt}), and tip speed (TS) can be found, which allows for the calculation of the rated wind speed (TS / TSR_{opt}) and the rated power. However, these three parameters are not calculated in a parametric manner since this model is set up for specific turbine types. Thus an adaption is needed to find the parametric rated wind speeds. This is done by implementing a Kriging meta-model trained on 11 diameters with known rated power in the range of 3-30 MW, with the methodology described in section 2.5. The meta-model takes the diameter as input and outputs a scaling factor that goes into the model to calculate the, now parametric, TS and TSR_{opt}.

The thrust curve is set up by a statistical approximation. This is achieved through a regression model for pitch-controlled wind turbines based on the available power and thrust curves of 72 wind turbines Atlaskin, Suomi, and Lindfors [3]. The thrust curve can be found by the correlation between the power curve, wind speed, swept rotor area, and air density. This equation and regression model from which the thrust curve can be found is given in Figure 4.2.

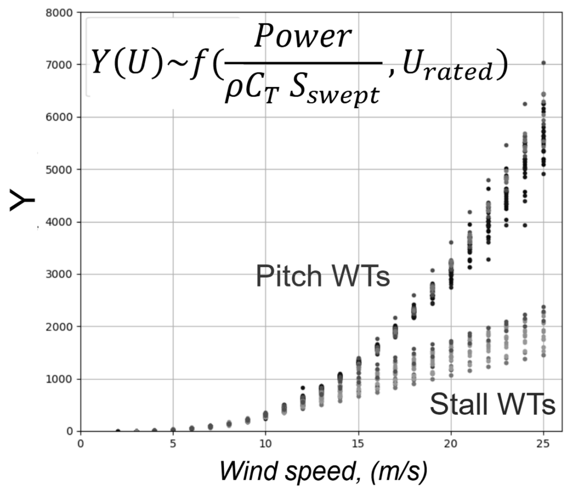

Figure 4.2: Correlation between the power and thrust curve Atlaskin, Suomi, and Lindfors [3]

However, the thrust curve also needs a scaling factor for the parameterization of investigated diameters since the statistical approximation is set up for 72 discrete turbine sizes. This is done for the same range of known diameters as the power curve by setting up a Kriging meta-model. The meta-model takes the diameter as input and gives the scaling factor for the thrust curve as output.

Both these Kriging meta-models are thus trained on 11 discrete points with a training-validation ratio of 80-20% which is a common division for machine learning models Morozova et al. [29]. The Kriging metamodels can be seen in Figure 4.3 for the range of 90-340 meters rotor diameter with the 95% confidence interval for each point. The best improvement point is also identified, this is the point where, when added to the training set of the Kriging meta-model, the largest increase in accuracy is gained. This point is found where the 95% confidence interval is the widest, which for both meta-models is the case for a rotor diameter of 312 meters. This would be the most logical point to add to the dataset if improvements are desired.

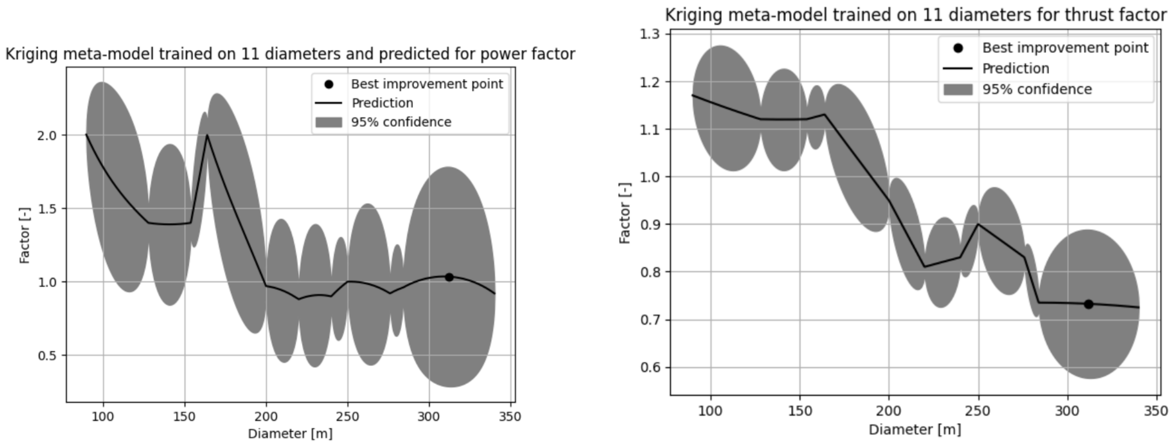

Figure 4.3: Kriging prediction and 95% confidence interval for power and thrust scale factors

Since for both the power and thrust curves the factors are only assumed certain for the discrete 11 points for which their respective meta-models are defined, it is important to quantify the uncertainty when a diameter between two discrete points is used. To account for these uncertainties, both the power and thrust scaling factor are implemented as a stochastic variable. Besides the scaling factors, Saint-Drenan et al. [35] has shown through their sensitivity analysis that there can be significant changes in the power curve if the turbulence intensity and air density are changed over an interval. Because of this, it is chosen to also incorporate these variables as stochastic variables for the MCS process in energy production. These variables will be modeled as beta-PERT distributions since they rely on historical data, with characteristics as displayed in Table 4.1.

The distributions for the scaling factors are centered around the prediction for a certain diameter and have a variance of prediction plus or minus the standard deviation from the meta-model at a specific diameter. The values for turbulence intensity are taken from Tai et al. [41], from validation of turbulence intensity simulation. The values for air pressure are taken from a study of air pressure differences over heights. The minimum is chosen to be the minimum density at 305 meters, the most likely the mean value at 0 meters, and the maximum the max value at 0 meters He et al. [16]. This illustrates the variance in air pressure between a large and a small turbine.

Table 4.1: Parametric variables parametric energy production

Stochastic variable	**Min**	**Most-likely**	**Max**
Scaling factor power [-]	prediction(D)-SD(D)	prediction(D)	prediction(D)+SD(D)
Scaling factor thrust [-]	prediction(D)-SD(D)	prediction(D)	prediction(D)+SD(D)
Turbulence intensity [-]	0	10	25
Air density kg/m^3	1.1088	1.2240	1.3152

Through these meta-models and the MCS, the parametrically calculated probabilistic power and thrust curves of all diameters between 90-340 meters can be generated.

4.2.2. Wakemodel

A wake refers to the turbulent flow region that occurs downstream of a solid object as it moves through a fluid. This phenomenon is caused by the fluid's motion around the body. In the case of wind turbines, the wake is caused by air flowing through and being disrupted by the rotor area. A wake is characterized by a reduction in mean wind speed and an increase in turbulence levels behind a turbine. The primary reason for accurately modeling wind turbine wakes is that wind turbines situated within wind farms experience altered inflow wind conditions compared to standalone turbines. This variation occurs due to the wakes generated upstream by other turbines. Therefore, wake models become crucial when multiple turbines are placed in close range to each other because they can mutually influence each other, potentially resulting in reduced energy generation. This research will focus on the wake models present in PyWake, which can be seen in Appendix A. Based on these graphs, different wake models can be used for different applications. The Bastankh Gaussian model is used for a wind farm-wide wake model. This model has decent wake deficit coverage both in profile and in distance.

4.2.3. Environmental modelling

The wind conditions are implemented by analyzing historical wind data, focusing on the frequency and directionality of wind from 12 equally divided sectors spanning 0 to 360 degrees. This wind data is represented using a Weibull distribution (subsection 2.6.1), with shape and scale parameters derived from the actual data. This distribution faithfully mirrors the real environmental conditions prevalent at the location. The environmental data is loaded into the model in the form of the 100m u and v-component of wind from the database ”ERA5 hourly data on single levels from 1940 to present”, which is publically available from the Copernicus satellite database.

4.2.4. wind farm layout

The initial layout and the number of turbines in the available plot are set up by a grid-based approach through the inter-turbine spacing. An algorithm is then used to place a certain amount of turbines in a user-defined plot based on the optimizable spacing and rotor diameter. This means that with a lower spacing and/or lower rotor diameter more turbines will be able to fit into the plot. With a higher spacing and/or rotor diameter the opposite is true.

With this initial grid-layout energy production and material use are determined. Figure 4.4 gives an example of how the wind farm layout is created for a user-defined plot.

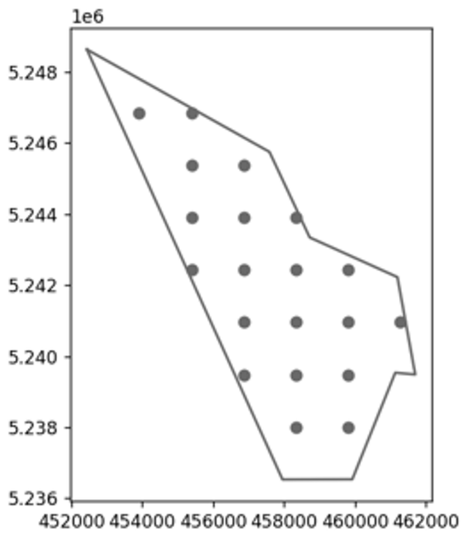

Figure 4.4: Example grid layout for wind turbines with diameter: 295m and inter-turbine spacing: 5 diameters

4.2.5. Output

The parametric energy production gives as output the total yearly energy produced by the simulated wind farm

4.3. Parametric material use

A wind farm consists of multiple structures and connections. One typically makes the distinction between the turbine and the balance of plant- (BoP) level. The turbines create electricity from the wind resource. From top to bottom, they generally consist of three rotors connected to a nacelle, a tower supporting the rotor nacelle assembly (RNA), and a foundation system, in the case of this research a monopile.

The BoP is the group name for all equipment, structures, and connections that serve the wind turbines. This usually consists of an offshore substation, array cables from the turbines to the substation, an export cable transporting the electricity from the offshore substation to shore, and an onshore substation. In this research, the onshore substation is left outside the scope.

4.3.1. RNA

The RNA consists of an array of machinery and parts. Even though Fingersh, Hand, and Laxson [14] can not be deemed as state-of-the-art, all the objects that an RNA is composed of are listed in great detail here, including their respective weights. This is used to find the RNA mass which forms the top mass of the tower and monopile. Since [14] is based on smaller turbines, the extrapolation to the larger turbines in this investigation gives an overestimation of the weights. This is a limitation of calculating the masses in this manner.

4.3.2. Foundation and tower

The tower and foundation need to be able to support the forces created by the RNA weight, the moment created by the thrust force of the rotor, the tower self-weight, and the monopile self-weight. The bending moment will be the largest at the tower bottom and monopile bottom and can be described by Equation 4.1.

$$M_{WT} = \frac{1}{2}\rho A_{\text{rotor}} V_{WS}^2 C_p * H \tag{4.1}$$

This subsection will explain how the weights of the monopile and the tower are parametrically determined, first through a force analysis and afterward by Kriging meta-modeling.

4.3.2.1 Force analysis

The tower and the monopile weight are calculated by determining their needed diameter for the forces that are exerted on the structure. The main forces are the axial downwards force due to the RNA, the axial downwards force of the tower and/ or monopile section above it, and the moment caused by the horizontal thrust force, calculated by Equation 4.1. These forces need to be counteracted by the cross-section such that the occurring stresses are below the tensile strength of the material, assumed as S355. In order to find the needed diameter to counteract these forces, a force analysis is performed based on top force and tower bending moment. This is done by calculating a tapered circular hollow section with the given forces and self-weights. From this, the diameter and/or steel volume is found Hernandez-Estrada et al. [17]. The equation for the force analysis can be seen in Equation 4.2. This analysis does not take the wave forces into account.

$$\sigma_{\max} = \frac{F_g}{A_b} \pm \frac{My}{I} \tag{4.2}$$

where,
F_g is the top load [kN]
A_b is the cross section area [m^2]
M is the bending moment [kNm]
y is the distance of the neutral axis in the cross-section [m]
I is the moment of inertia of the cross-section [m^4]

by assuming that there is a correlation of $t = \frac{D}{200}$, the diameter can be isolated outside of the area and moment of inertia and solved for. When the diameter is isolated, a function is set up that discretizes the tower in N sections and calculates the needed diameter to stay under the tensile strength divided by the safety factor of 1.15. By using a high number of N, each cross-section diameter can accurately be calculated for the RNA weight, self-weight, and moment occurring at that given slice. In the end, the steel volume is calculated based on all individual diameters, thicknesses, and tower height.

For the monopile, the same is valid as for the tower. The difference is that an even larger moment and axial force act upon the monopile than the tower since the water depth is added as extra height to Equation 4.1. Besides this, the monopile also needs a certain penetration depth to keep the wind turbine stable. This penetration depth can be calculated by Equation 4.3 according to Srikanth et al. [39].

$$L = 56.52 - 1.397 * SA + 1.138 * I \tag{4.3}$$

Where,
L is the needed penetration depth of the monopile [m]
SA is the angle of internal friction of soil [deg]
I is the moment of inertia of the monopile [m^4]

The thrust force that causes the bending moment is calculated with the parametric power and thrust curves as explained in section 4.2. This is done by finding the rated speed through TSR_{opt} and TS and by using the maximum thrust coefficient.

4.3.2.2 Kriging meta-model

Besides the force analysis method, a prediction based on formerly executed high-fidelity calculations is implemented. This is done through a Kriging meta-model trained on 4 diameters with rated power in the range of 15-22 MW, with the methodology described in section 2.5. Through this method, the monopile diameter thickness and length and the tower base and top diameter and tower length are determined. This has the added advantage of knowing the section dimensions with quantified uncertainty. Since these meta-models are trained on high-fidelity calculations, this analysis does take the wave forcing into account.

These Kriging meta-models are thus trained on 4 discrete points with a training-validation ratio of 80-20% which is a common division for machine learning models Morozova et al. [29]. The Kriging meta-models can be seen in Figure 4.5 and Figure 4.6 for the range of 15-22 MW for the monopile diameter, tower diameters and tower length and 30-70 meters of water depth for the monopile length with the 95% confidence interval for each point. The best improvement point is also identified, this is the point when added to the training set of the Kriging meta-model, the largest increase in accuracy is gained. This point is found where the 95% confidence interval is the widest. For the meta-models trained on the rated power, this best addition point would be 16.5 MW. For the meta-model trained on water depth, the point would be 65 meters of water depth. These would be the most logical points to add to the dataset if improvements are desired.

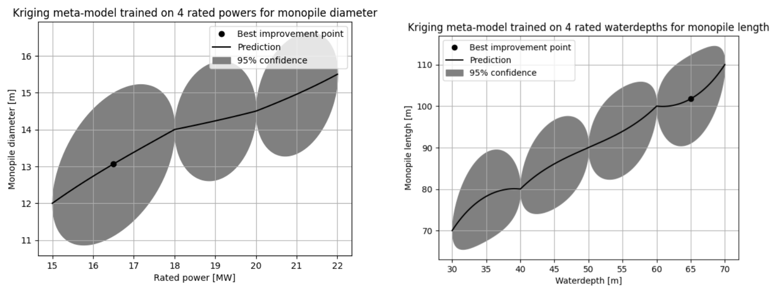

Figure 4.5: Kriging prediction and 95% confidence interval for monopile diameter and length

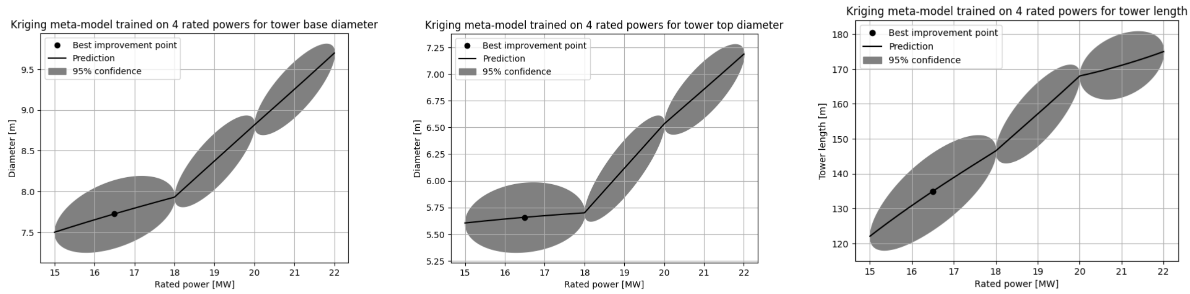

Figure 4.6: Kriging prediction and 95% confidence interval for tower diameters and length

It is chosen to incorporate the air density, monopile diameter, monopile thickness, monopile length, tower base diameter, tower top diameter, and tower length as stochastic variables for the MCS process in the material use since these variables are most prone to slight variations. These variables will be modeled as beta-PERT distributions since they resemble expert judgment and historical data [section 2.6] with characteristics as displayed in Table 4.2.

The values for air pressure are taken from a study of air pressure differences over heights. The minimum is chosen to be the minimum density at 305 meters, the most likely the mean value at 0 meters, and the maximum the max value at 0 meters He et al. [16]. This illustrates the variance in air pressure between a large and a small turbine. For all outputs from the meta-model, the most likely value is the prediction for a certain diameter and the variance is this prediction plus or minus the standard deviation at this diameter.

Table 4.2: Stochastic variables parametric material use

Stochastic variable	Min	Most-likely	Max
Air density kg/m^3	1.1088	1.2240	1.3152
monopile diameter [m]	prediction(D)-SD(D)	prediction(D)	prediction(D)+SD(D)
monopile thickness [m]	prediction(D)-SD(D)	prediction(D)	prediction(D)+SD(D)
monopile length [m]	prediction(D)-SD(D)	prediction(D)	prediction(D)+SD(D)
towerbase diameter [m]	prediction(D)-SD(D)	prediction(D)	prediction(D)+SD(D)
towertop diameter [m]	prediction(D)-SD(D)	prediction(D)	prediction(D)+SD(D)
towerlength diameter [m]	prediction(D)-SD(D)	prediction(D)	prediction(D)+SD(D)

4.3.3. Substation

An offshore substation consists of a substation containing the transformer and other equipment and a foundation carrying this topside. According to Buchan [7], the topside mass of substations and the mass of jacket foundations can be approximated as seen in Table 4.3 and Equation 4.4 based on its total rated power in the wind farm.

Table 4.3: Topside mass approximations

Topside [MW]	Mass assumed [t]
400	2300
500	2700
600	3000
700	3200

$$M_{found} = X\frac{H^2}{2} + Ym_{ts}H + Z \tag{4.4}$$

where,
M_{found} is the foundation mass [t]
X is the slope factor = 1 [-]

H is the water depth [m]
Y is the slope factor = 0.004
m_{ts} is the topside weight [t]
Z is the jacket weight factor = 750 [t]

This table and equation are set up by fitting the factors to data from the 4C database (Buchan [7]).

The topside mass is found by first calculating the wind farm rated power. This is done by multiplying the individual turbine-rated power with the number of turbines from the parametric energy production. This total wind farm-rated power is then used to calculate the topside mass through an interpolated function set up by Table 4.3. With the topside mass, the support structure mass is found through Equation 4.4. From this, the topside and support structure mass are known.

4.3.4. Cables

The material used for the cables is given by Li et al. [25] and summarized in Table 4.4.

Table 4.4: Material use for array and export cables

Cable type	Weight [t/km]
Inter-array [66kV]	26.4
Export-cable [132kV]	74

The turbine locations are according to the grid set up in parametric energy production and it is assumed that the substation will be in the middle of the wind farm. The export cable length is found by the minimal distance from the middle of the wind farm to the boundary plus the offshore distance. It is assumed this boundary is also closest to shore.

4.3.4.1 Optimization

According to the internal "Optimal wind farm cable routing" model, the optimal array cable length is found by creating all possible networks given the power rating of the cable type and the rated power of an individual turbine. The cable power rating is calculated by Equation 4.5

$$P_{rated} = V * 1000 * I_c * 3^{0.5} \tag{4.5}$$

where,
P_{rated} is the cable rated power [kW]
V is the array cable voltage (either 33 or 66 kV) [kV]
I_c is the current (800A) [A]

Based on the power rating of the cable and the turbine power rating, a certain amount of turbines can be connected per cable. model finds the minimum total length to connect all the turbines and returns this value.

4.3.4.2 K-means

Besides the optimal array cable length, a faster approach is also incorporated which calculates a preliminary cable length. This is done by partitioning the wind farm through a K-means algorithm based on the amount of cables needed to connect all wind turbines. When the clusters of turbines that can be serviced by a single array cable are identified, a network is constructed through NetworkX to find the minimum distance needed to connect all turbines in a cluster to the substation. This is done for all clusters and the cable length is added together to find the total array cable length.

4.3.5. Output

The parametric material use gives the total weight of the rotor and nacelle, the weight of the tower, the weight of the monopile, the weight of the substation topside, the weight of the substation jacket, the array cable length and the export cable length as output.

4.4. Fatigue surrogate modeling

To find the parametric wind turbine fatigue, a surrogate model is set up using openFAST. This section will discuss the steps that were taken to end up with a stochastic parametric fatigue model which predicts fatigue for seven design variables and gives the expected modeling error interval.

4.4.1. openFAST surrogate

OpenFAST is a multi-physics, multi-fidelity tool for simulating the coupled dynamic response of wind turbines. It is a robust and versatile numerical modeling tool suited for analyzing the performance and structural integrity of offshore monopile wind turbines across various environmental conditions. Practically speaking, OpenFAST is the framework (or glue code) that couples multiple specialized modules, each crucial for simulating different aspects of wind turbine behavior. TurbSim, for instance, generates realistic wind fields, while HydroDyn accurately models hydrodynamic forces acting on the turbine structure in marine environments. The ElastoDyn module enables the precise representation of the turbine's structural dynamics, essential for assessing fatigue damage accurately. Additionally, AeroDyn simulates aerodynamic loads on the blades, and ServoDyn ensures realistic control system behavior. Together, these modules provide a comprehensive framework for assessing the complex interactions between wind, waves, and turbine dynamics, making openFAST a suited choice for studying fatigue damage in offshore monopile wind turbines under varying environments.

4.4.1.1 Input

The input for openFAST will form the basics for the surrogate model. The different variables that will be varied are thus important to the degree of parametric fatigue behavior. The variables that are varied for a single turbine (with specific rotor diameter and monopile size) can be seen in Table 4.5, including the range they are varied over and the number of discretizations in this range.

Table 4.5: The varied input variables to create a parametric surrogate model through openFAST

Variable	**minimum value**	**maximum value**	**number of disrectizations**
Wind speed [m/s]	3	25	4
Wind direction [°]	-90	90	3
Turbulence intensity [-]	0.0005	30	4
H_s [m]	1	11	3
T_p [s]	1	9.71	3
Wave direction [°]	-90	90	3
Current speed [m/s]	0.25	0.25	1
Current direction [°]	0	360	1
Probability [-]	1	1	1

The wind speed, H_s, T_p, and wave direction correspond to environmental conditions. The turbulence intensity reflects the design variable spacing of turbines since this can be calculated by Equation 4.6 Shariff and Guillou [37].

$$I_+ = a(x/D)^{-b} \quad \begin{cases} a = 0.16C_T^{4.83} + 0.179 \\ b = 0.68I_a + 0.472 \end{cases} \tag{4.6}$$

where,
I_+ is the added turbulence intensity due to a turbine [-]
x is the turbine spacing [m]
D is the rotor diameter [m]
C_T is the thrust coefficient [-]
I_a is the ambient turbulence intensity [-]

The wind direction reflects the misalignment of the turbine with the wind, where 0 is the rotor plane perpendicular to the wind direction and 90/ -90 is the rotor plane parallel to the wind direction. This does not have a high enough discretization to incorporate wake steering, but can only turn the rotor out of the wind. Besides, taking multiple turbines with different rotor diameters can reflect the design parameter of rotor diameter.

4.4.1.2 High performance computing methodology

These different input variables are varied until each unique load case is created with distinct conditions. In total, this creates 1296 load cases per wind turbine. For each load case, multiple operations are executed to represent this load case in the standard openFAST input files:

1. Wind speed and turbulence are changed in the turbsim input, creating the wind field.
2. The wind direction is adapted in the InflowWind file.
3. the H_s, T_p, and wave direction are changed in the HydroDyn file.

Finally, The current speed and direction are kept equal since this does not cause a large tower bending moment which is assessed for fatigue. Probability is set at 1, which means the presented load-case occurs in the simulation.

With these adapted inputs, each input is run for a full hour of simulation time, to ensure the statistical field is large enough such that random seeds are not necessary. This is done through a High Performance Computing (HPC) batch-job command which can handle 127 simulations simultaneously. Multiple bash scripts are written and utilized for the whole input process. The most important scripts in the input phase handle:

- writing all the different load-cases
- copying and altering all the different openFAST input files to create all the simulation directories
- running 127 simulation directories simultaneously and waiting until these are complete before running the next batch
- Checking if all simulations were successful in the end and otherwise identifying troublesome directories and re-simulate these

These scripts highly automate the process, even though it still forms a lengthy process that takes a few days to simulate.

The selected output from openFAST is the tower bending moment in the x and in the y direction at the tower bottom. This will be used to calculate the fatigue in the tower, which is deemed a significant fatigue hot spot suitable for comparison between different turbine configurations.

4.4.1.3 Fatigue calculation

With the tower bending moment in two directions, the tower fatigue can be calculated at the tower bottom. This is done by first converting both moment time series into a stress time series. This is done through Equation 4.7

$$\sigma = \frac{D * M_x}{I} + \frac{D * M_y}{I} \tag{4.7}$$

Where,
σ is the occurring stress in the cross-section [N/m^2]
D is the tower diameter [m]
M is the bending moment in x and y direction [Nm]
I is the moment of inertia of the cross-section [m^4]

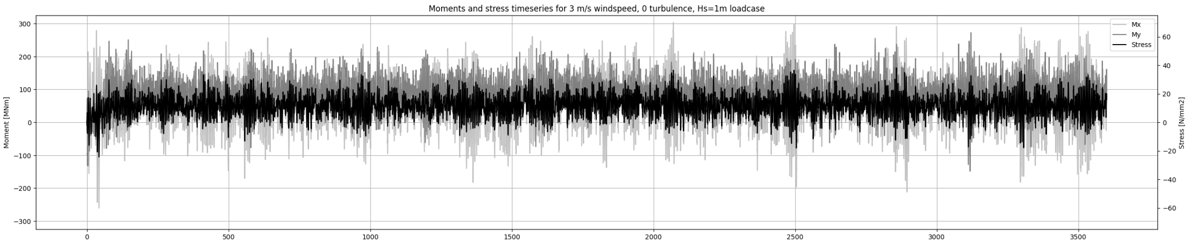

Figure 4.7: Moment and stress one-hour timeseries

This stress time series, of which an example is given in Figure 4.7, is then put through a rain-flow counting algorithm which bins the different stress ranges with a certain occurrence. From here, two arrays are returned. An array containing the present stress ranges and an array of how often these specific stress ranges occur in the time series. This is used to calculate fatigue.

The equations described by Equation 2.10 and Equation 2.11 are written into Equation 4.8 by using log-rule and adjusting for specimen thickness.

$$\log(N_{\sigma,occur}) = \log(a) - m\log_{10}(\text{deltaF}) - m\log_{10}\left(\frac{t_{\text{tt}}}{t_{\text{ref}}}\right)^{k} \tag{4.8}$$

Where,
$N_{\sigma,occur}$ is the fatigue cycle life for the occurring stress ranges [number of cycles]
a, m, and k are material-specific constants obtained from experimental data or SN curves. [-]
deltaF is the stress range (amplitude) of the cyclic loading, found through the rain-flow algorithm [N/m^2]
t_{tt} is the thickness of the cross-section (assumed as 0.08m) [m]
t_{ref} is a reference thickness (taken as 0.025m) [m]

This equation is adapted for high-cycle and low-cycle fatigue. For high-cycle (N > 10^4 cycles) the material-specific values a and m are different than for low-cycle fatigue based on the difference between Basquin and Coffin's fatigue approaches. Through this adjustment, the fatigue calculation is suitable for a wide range of loading conditions.

With the fatigue cycle life calculated, the fatigue damage over a lifetime can be calculated by Equation 4.9

$$D_F = \frac{n_{\sigma,occur} * factor_{lifetime}}{N_{\sigma,occur}} \tag{4.9}$$

Where,
D_F is the lifetime fatigue damage which needs to be < 1 to not fail [-]
$n_{\sigma,occur}$ are the number of cycles for the occurring stresses in the time series, counted by the rain-flow algorithm [number of cycles]
$factor_{lifetime}$ is the factor that converts the time series into lifetime (1 hour to N years) [hour]

It is important to note that the extrapolation to lifetime fatigue is only possible when the simulated time series is representative of the lifetime loading conditions. However, since the main purpose is comparing design variants, this is assumed acceptable here.

This fatigue damage is calculated for all 1296 different load cases per wind turbine.

4.4.1.4 Output

The output from the openFAST surrogate model is the lifetime fatigue damage for all 1296 different load cases per turbine type. In the case of this thesis, the only turbine included is the IEA15MW, which is deemed representative of the investigated diameters but, a true parametrization for the diameter is thus not possible.

4.4.2. Kriging meta-model

The openFAST surrogate model is now in the form of a large data frame with all the discrete load conditions with their respective fatigue damage. The goal is to create a continuous surrogate model for the load conditions where the predicted output is provided with a level of uncertainty when predicting between discrete inputs. This is achieved by setting up a seven-dimensional Kriging meta-model.

4.4.2.1 Kernel optimization

To find the most accurate hyperparameters, the observed data from openFAST is separated into a training and validation dataset of 80 and 20 percent of the data respectively. Since the surrogate model has 7 dimensions (seen in Table 4.5 and diameter), 7 kernels will need to be constructed with their hyperparameters. As described in section 2.5, it is chosen to use the openTURNS squared exponential as this kernel. The individual θ needs to be set up for each variable. This θ gives information about the statistical dependencies between observations. These hyperparameters are determined using the minimization of the MSE as described in subsection 2.5.2.

4.4.3. Output

The output for the fatigue Kriging meta-model is lifetime fatigue for a certain design variant, including the uncertainty that follows from creating a continuous surrogate model from discrete sample values. Due to the seven dimensions, it is not possible to visualize the surrogate model.

4.5. Parametric vessel use

As can be seen in Appendix B, a certain vessel fleet is necessary for the different life-cycle activities of the wind farm. These activities are modeled by the linear planning tool NetworkX. With this simulator, it is possible to create a realistic network of activities where dependencies, parallel activities, and sequential activities can be modeled. The turbine construction, cable construction, maintenance, and decommissioning networks that are modeled in NetworkX will schematically be explained in this section.

4.5.1. Turbine construction

For the construction of the turbines, the monopile foundation and jack-up vessel need to be transported to the site by tugs and barges first. On site, these foundations are then installed by the jack-up vessel, after which the barges and a tug return to pick up the pump, rocks, and turbine. One tug stays to relocate the jack-up vessel later. When the pump has arrived, grout is pumped into the freshly installed foundation fixing it in place. After this, the barge with rocks will place the scour protection. Finally, the tugs with the jack-up and turbine will move back to the installed monopile to install the turbine. After this, the tugs return to shore to start the cycle for a new turbine. This complete process can be seen in Figure 4.8 and is modeled in this manner in NetworkX.

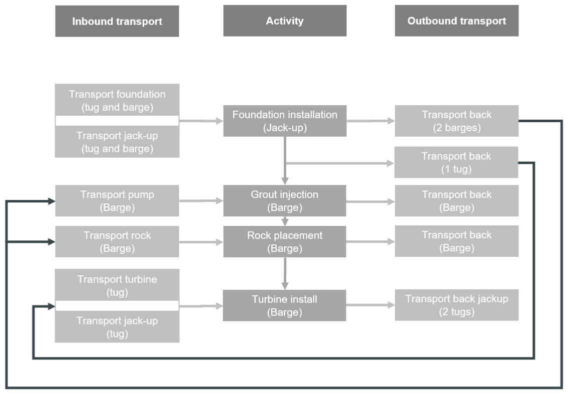

Figure 4.8: The network for turbine installation

4.5.2. Cables construction

The cable installation starts with two tugs transporting a jack-up vessel to the substation location and the moving of a dredge and AHV to the site. The jack-up vessel will install the substation, while in parallel the AHV is clearing the sea-bottom route and the dredge is dredging the route for the cable. After this, all these vessels move back to shore. Next, a plough-vessel and two OSVs move to the site in anticipation of the array cable laying by the plough vessel while the OSVs support the process. After this, the plough-vessel and OSVs move back to shore while a rock barge is on its way to place the rock on the installed array cable as protection. After placing the rock, the rock barge moves back to shore to pick up more rock for the export cable. The plough-vessel has picked up the export cable from shore and is now on its way back to install. When the export cable is installed, the rock barge is back with new rock to place over the export cable for protection. The plough-vessel moves together with an OSV to the shore landing. At the shore landing, the OSV and plough-vessel install the landing cable. Then they return to port. This complete process can be seen in Figure 4.9 and is modeled in this manner in NetworkX.

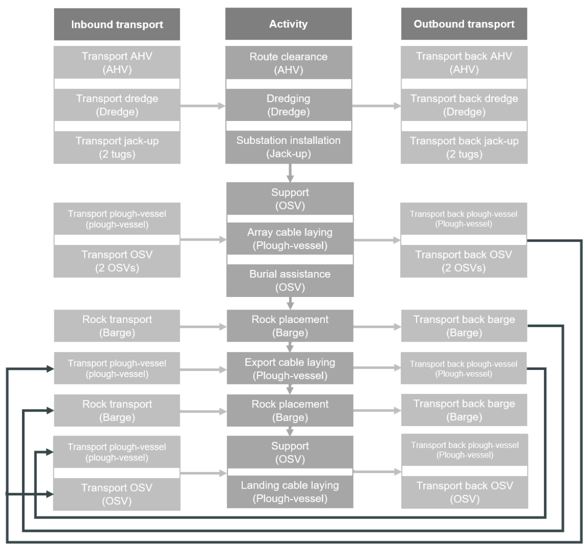

Figure 4.9: The network for cable installation

4.5.3. Maintenance

The maintenance procedure consists of two main categories. An OSV inspects the turbines, cables, and substation in sequence for the planned maintenance. For this part, there need to be enough OSVs in the fleet to be able to do these inspections in a one-year timeframe. Secondly, there can be incidental maintenance. This is when something breaks and there needs to be an incident inspection and specific repair afterward. The incident maintenance is also handled by an OSV, after which this OSV together with a jack-up transported by two tugs either needs to replace the nacelle, blades or repair small components. These incidents are dependent on the fatigue resistance of the structure and are therefore related to the fatigue component of the model. In the end, the fleet size for maintenance needs to be large enough to be able to handle the planned maintenance. The complete process can be seen in Figure 4.10 and is modeled in this manner in NetworkX.

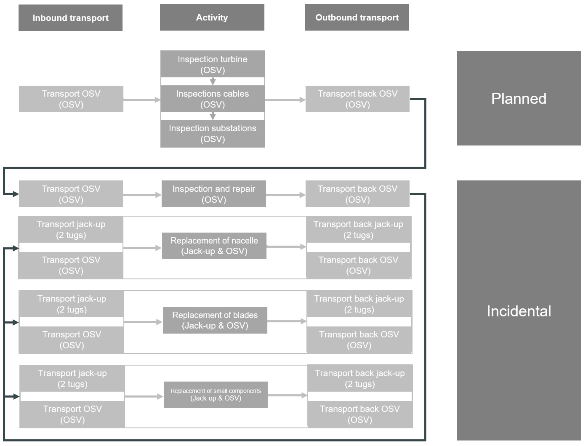

Figure 4.10: The network for maintenance

4.5.4. Decommissioning

At the end of life, decommissioning of the turbines needs to take place. This process is quite complicated when also looking at the shore-side decommissioning. For this analysis, this phase is simplified by only looking at the offshore aspect. A jack-up is transported by two tugs after which a turbine is disassembled. After this, the jack-up is tugged back to shore and the cycle for one turbine is repeated for all turbines. This process can be seen in Figure 4.11 and is modeled in this manner in NetworkX.

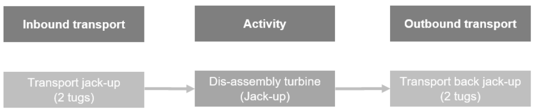

Figure 4.11: The network for decommissioning

4.5.5. Uncertainty

The durations from Appendix B are adapted for the network construction. However, there can be a significant difference in small and large wind turbines' construction, maintenance, and decommissioning. For this reason, the work times are modeled as stochastic variables whereby an activity can take 25% less time or 50% more time. These decreases and increases are assumed to be reflecting real work times in a better manner. These stochastic variables are then used for the MCS in to quantify the uncertainty. These variables will be modeled as beta-PERT distributions with characteristics as displayed in Table 4.6.

Besides this, it is important to note that the transport times found in Appendix B are not being used since these are calculated based on user-defined vessel speeds and offshore distance.

Table 4.6: Parametric variables parametric vessel use

Stochastic variable	Min	Most-likely	Max
Construction of foundation [h]	18	24	36
Injection of grout [h]	18	24	36
Dumping of rock [h]	21.75	29	43.5
Assembly of wind turbine [h]	18	24	36
Substation installation [h/km]	6	8	12
Dredging [h/km]	18	24	36
Route clearance [h/km]	2.43	3.24	4.86
Array cable laying [h/km]	18	24	36
Support [h/km]	18	24	36
Burial assistance [h/km]	18	24	36
Rock placement [h/km]	1.5	2	3
Export cable laying [h/km]	2.65	3.53	5.3
Rock placement [h/km]	1.5	2	3
Landing cable laying [h/km]	1.2	1.6	2.4
Support [h/km]	3	4	6
Regular inspection turbine [h]	45	60	90
Regular inspection cables [h]	252	336	504
Regular inspection substation [h]	135	180	270
Irregular inspection and repair [h]	0.36	0.48	0.72
Replacement of nacelle or blades [h]	18	24	36
Replacement of small component [h]	0.36	0.48	0.72
Dis-assembly of turbine [h]	9	12	18

4.5.6. Output

After modeling all the different phases, there is a difference in the project duration and the total ship duration. Since multiple activities are executed simultaneously, the project duration is smaller than the total ship duration. This difference becomes even larger when the fleet size is increased, where ship duration will increase but project time decrease. In the end, the output is given as the project duration and ship duration. The project duration strongly influences the financial gain. The shorter the project, the more production time during the lifetime. On the other side, the ship duration influences the CAPEX, OPEX, and sustainability by the day rates and fuel usage.

4.6. Objectives

With the parametric calculations of energy, material use, fatigue, and vessel use it is possible to build the objective functions. The objective functions translate the technical capabilities with the socio-economic desire abilities of the model user. This is done through the objective functions that quantify the sustainability score, the total annual energy production (AEP), the capital expenditure (CAPEX), the operational expenditure (OPEX), the fatigue, and the meta-model uncertainty. For this, the probabilistic outcomes of the design performance functions are simplified to the most likely value by taking the mean for the objectives. This makes the optimization possible.

4.6.1. Sustainability

The sustainability objective combines the vessel use and the material use design performance functions to create outputs based on a specific design variant for the sustainability objective. To translate these two design performance functions into the sustainability objective output, first, the materialistic composition of different parts of the wind farm and the fuel consumption of the fleet will be investigated. After this, these two drivers will be translated into six different sustainability scales by using the Idemat eco-costs database *Data,Tools,Books* [10]. The end-user can then choose what scale to use for the model optimization.

4.6.1.1 Material composition

First, the material composition of the cables, substation, and turbines is investigated. Material compositions for the cables and turbines are given by Li et al. [25] and Li et al. [26] respectively. For the substation, it is assumed the topside has the same material profile as the nacelle and the support structure the same as the monopile. The material composition of the cables is given in Table 4.7 and the composition of the turbine and substation in Table 4.8

Table 4.7: Material composition for array and export cables

Material type	Inter-array [66kV]	Export-cable [132kV]
Copper [%]	22.6	27.0
Polyethelene [%]	6.2	8.7
Lead [%]	26.2	25.0
High-alloy steel [%]	41.0	35.0
Polypropylene [%]	4.2	4.9

Table 4.8: Material composition for turbine and substation

Material type	Permanent magnet drive	Fiberglass rotor	Carbon fiber rotor	Steel tower	Monopile	Substation support structure	Substation topside
Iron [%]	52.6	25.8	25.8	0	0	0	52.6
High-alloy steel [%]	29.8	9.4	9.4	0	0	0	29.8
Low-alloy steel [%]	8.9	9.8	9.8	97.1	100	100	8.9
Copper [%]	7.8	0.1	0.1	1.9	0	0	7.8
Aluminum [%]	0.9	0.1	0.1	1.0	0	0	0.9
Glass fiber [%]	0	37.3	0	0	0	0	0
Carbon fiber [%]	0	0	41.7	0	0	0	0
Resin [%]	0	17.5	13.7	0	0	0	0

4.6.1.2 Fuel consumption

For the life cycle activities, a certain fleet is necessarily composed of multiple ships. These ships also have varying fuel types and consumption. This fuel consumption can be found through Li et al. [25] and are summed up in Table 4.9

Table 4.9: Material composition for array and export cables

Ship type	Fuel type	Fuel rate [kg/h]
Tugboat	Diesel	268.4
OSV	Diesel	218.4
Jack-up	Heavy fuel oil (HFO)	167.1
Barge	HFO	153.9
Dredge	HFO	98.3
AHV	HFO	98.3
Plough-vessel	HFO	98.3

4.6.1.3 Material sustainable cost

With the specific material composition and fuel consumption known for the full wind farm lifetime, the sustainability can be calculated towards nine known sustainability scales. Five of them calculate the associated cost of using a kilo of material on human health, exotoxicity, resource scarcity, carbon footprint, and a combined eco-cost.

Three scales use the ReCiPe method to define the impact of the use of materials on human health, eco-toxicity, and resource scarcity. The units of these scales are the years that are lost or that a person is disabled due to a disease or accident (DALYs) for human health, the local species loss integrated over time (species loss/year) for exo-toxicity and the extra costs involved for future mineral and fossil resource extraction ($) for resource scarcity Huijbregts et al. [20]. These three scales can give an in-depth picture of the impact of certain constructions on the environment.

The final scale gives the amount of CO_2/kg of material used and therefore gives the carbon footprint. Through these nine scales, the user can always find a sustainability scale most suitable for the current design question. The cost values for the materials are shown in Table C.1 for the first five and in Table C.2 for the last four scales.

4.6.2. AEP

The AEP is calculated by subtracting the energy losses due to power transmission from the energy production. The power loss is calculated using Equation 4.10 Lerch, De-Prada-Gil, and Molins [24].

$$P_{\text{loss,x}} = 3\left(\frac{P_{\text{gen}} + P_{\text{trans}}}{\sqrt{3} * V}\right)^2 * R_{\text{cable}} * L_{\text{cable,x}} \tag{4.10}$$

Where:
P_{gen} is the power generated by the wind turbine that is being connected at point x [MW]
P_{trans} is the power already being transmitted through the cable from the previously connected turbines [MW]
V is the cable voltage [kV]
R_{cable} resistance of the cable [Ω]
$L_{\text{cable,x}}$ is the length of the cable at point x [m]

With this formula, the array cable lengths are being discretized based on the amount of connections that each cable has. The power going through the cable will thus increase over distance and the same holds for the energy losses. For the export cable, the whole energy production is placed on the cable from the beginning thus a discretization of the cable is not necessary. With all the energy losses of the array cables and export cables known, the AEP including the energy loss can be calculated.

4.6.3. CAPEX

The CAPEX is calculated based on the cost drivers found in Table 4.10 Shafiee, Brennan, and Espinosa [36].

Table 4.10: CAPEX cost drivers and contributors

Cost driver	**Main cost contributors**
Development and project management	Rated power
Nacelle	Weight and electronics cost
Rotor	Weight
Tower	Weight and steel cost
Export cable	Length and export cable price
Array cable	Length and array cable price
Foundation	Weight and steel cost
Substation	Weight foundation and topside; costs steel and electronics
Installation	Duration vessels and dayrates
Decommissioning	Duration vessels and dayrates

To calculate the CAPEX, the user should define the costs as defined in Table D.1. For now, the table contains preliminary values. These values are then multiplied with the amount of needed material and vessel time.

4.6.4. OPEX

The operational expenditure is calculated based on the cost drivers found in Table 4.11 Shafiee, Brennan, and Espinosa [36].

Table 4.11: OPEX cost drivers and contributors

Cost driver	Main cost contributors
Operations	Maintenance fleet and day rates
Maintenance	Amount of maintenance events, maintenance ships, dayrates

The amount of maintenance events is based on the component reliability. To generalize the component reliability and find the occurring maintenance events, a maintenance simulator is created based on fatigue damage. The yearly fatigue damage is calculated by sampling from a Weibull distribution to find the windspeed, from a Jonswap to find Hs and Tp, and from a beta-PERT to find the wave heading. It is assumed these sampled environmental conditions represent reality. With this fatigue damage, it is checked for each turbine if maintenance is necessary. This is done by multiplying the fatigue damage with a safety factor of three and using it as a binomial probability. In other words, the fatigue damage with safety factor represents the probability maintenance needs to occur that year. If due to this probability maintenance needs to occur for a turbine, its fatigue damage is reset to 0 due to the executed repair. If maintenance does not occur for a turbine, the new yearly fatigue damage is determined from the distributions and accumulated to the previous damage. This is now the new probability maintenance needs to occur this year. This process is repeated for all turbines for all years in their lifetime. This gives the total amount of needed maintenance events over the lifetime, which can be calculated back to yearly maintenance events by dividing by lifetime. Figure 4.12 illustrates the process that takes place in the maintenance simulator.

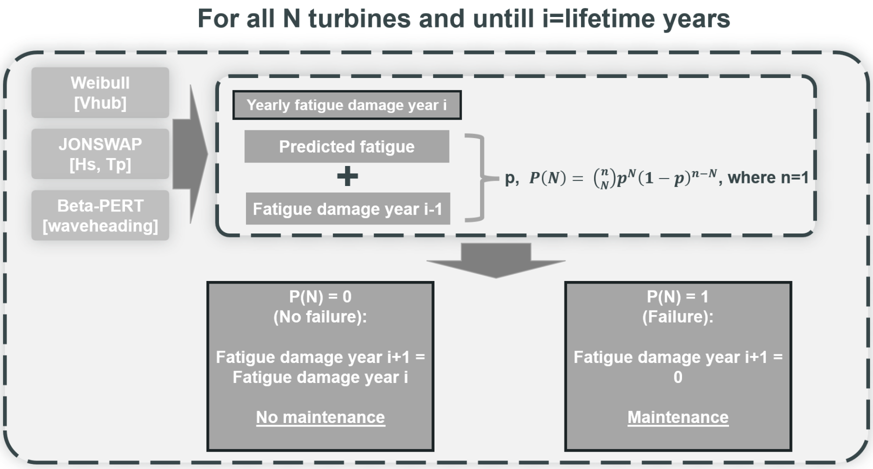

Figure 4.12: Illustration of maintenance simulator dependent on yearly fatigue damage.

4.6.5. Lifetime fatigue

The lifetime fatigue damage is a technical objective function that calculates the fatigue of the turbines over their entire lifetime without any economic components attached to it. It works in the same manner as the OPEX maintenance simulator, with the distinction that the yearly fatigue keeps increasing to the lifetime fatigue, and no binomial simulation is used to predict needed maintenance.

4.6.6. Fatigue meta-model uncertainty

The fatigue meta-model uncertainty calculates the degree of uncertainty of the fatigue meta-model for the specific variants. It is calculated as the coefficient of variation according to Equation 4.11

$$CV = \frac{standarddeviation}{mean} \tag{4.11}$$

This gives the level of accuracy of the prediction on a scale of 0 to 1. Here, 0 is the most and 1 is the least accurate.

4.7. Preference curves

To connect the user preference to the objective functions, preference functions are vital. subsection 2.2.3 describes the basic theory behind preference function modeling and how to set up a preference curve. These preference curves are defined in the optimization model under the ”preference functions” module. Through this, the user can create different types of preference functions such as a signal, triangular, beta-PERT, parabolic, and normal distribution. For each function, only three x-points need to be identified: the lower bound, the mode (where the score is highest), and the upper bound. The linear curve is created through the triangular curve by either setting lower bound = mode (a decreasing curve) or upper bound = mode (an increasing curve). With this, the preference functions are automatically generated. For simplicity, only linear and/ or triangular preference curves will be used in this thesis.

5

Verification

In the verification, the quality and accuracy of the generated data from the design performance functions are tested before the functions are used to generate results. This is done by using reference projects from which certain model outcomes can be found. It can be checked if the model gives the same or to a certain extent similar results as the reference project by adapting the model with variables that characterize these reference projects. In the case the results are similar enough, it can be said that the model is verified.

5.1. Energy production

5.1.1. Power and thrust curves

In order to check the similarity in energy production, the comparison of the power and thrust curves is highly important since this is the fundamental driver of the production. The power and thrust curves in the model are calculated according to section 4.2. Since this is based on Kriging meta-models, the power and thrust curves are accurate between the range of 3 to 30MW turbines. In Figure 5.1 the parametric calculation is performed through an MCS with a sample size of 1000. Here, the diameter is the same as real turbines of which the curves are known. This figure shows the comparison between the power and thrust curve of the known measurements and the output of the parametrically calculated power and thrust curves. It can be seen that these curves are very similar. The first main difference is that the calculated power curve slightly underestimates the total power through a higher decrease at rated windspeed due to increased turbulence assumptions. Secondly, the calculated power curve assumes a more conservative cut-out wind speed (the wind speed where the turbine stops producing) when compared to reality where this production decreases over a cut-out range. Lastly, the calculated thrust curve can be seen to be lower than the actual one for windspeeds under rated wind speed. This reduces the thrust and wake effect at sub-production windspeeds which has minimum effects on the total production on a windfarm scale. Altogether it can be said that the parametric generated power and thrust curves are slightly more conservative when compared to reality.

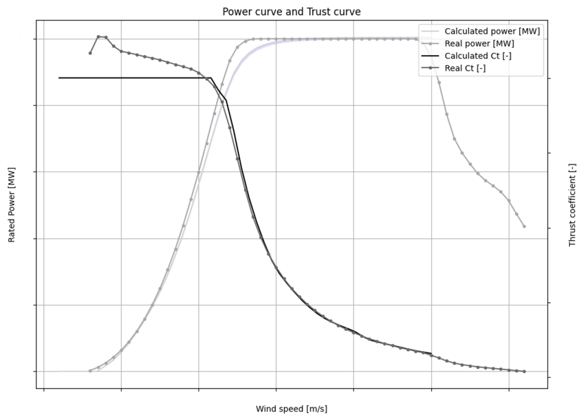

Figure 5.1: Comparison between the parametrically generated and a real power curve. Due to confidentiality the scales are redacted

5.1.2. AEP

The AEP is calculated through the parametric power and thrust curve as described in section 4.2 using an existing TotalEnergies' wind farm for the turbine locations, types, and wind conditions. In essence, the production of this wind farm is being simulated in order to compare it to real production. The real production of a wind farm is calculated through Equation 5.1.

$$AEP = N_{WT} * 24 * 365 * P_{rated} * CF \tag{5.1}$$

Where,
AEP is the annual energy production [MWh]
N_{WT} is the number of wind turbines [-]
P_{rated} is the rated power of one wind turbine [MW]
CF is the capacity factor: the factor which is windfarm specific and relates the theoretic to the real production. Usually, this factor is calculated after a representative year of production [-]

Due to confidentiality, these key performance indicators can not be disclosed. But when comparing the real production to the simulated one with the same boundary conditions, it is found that the simulation has a 6.40% lower AEP. Since this difference is conservative for energy production, it is deemed acceptable for the production as long as the user is aware of it.

5.2. Material use

It is challenging to quantify the true material use of existing wind farms since this data can be used to calculate the exact financial value of an asset, which can give a commercial advantage to competitors when known. For this reason, the two main contributors to the material use design performance function are verified in this paragraph: the material use for the foundations (which is directly correlated to all the weight it has to carry from the turbine on top) and the material use of the array cables (which is directly proportionate to the turbines rated power, their placement within the wind farm and the windfarm size).

5.2.1. Foundations

The foundations can be calculated through the preliminary design method using force analysis and the Kriging meta-model trained on internal data of previously executed projects as described in subsection 4.3.2. The Kriging meta-model has been trained on monopiles for turbines of 15 to 22 MW with a water depth of 30 to 70 meters. For these ranges, the Kriging meta-model is accurate at calculating the necessary foundation and wind turbine tower sections and lengths. Outside of this range, the meta-model extrapolates to find the foundation and tower sections and uncertainty increases. The force analysis method has been compared to the results of Damiani, Dykes, and Scott [9] where the monopile mass of a 5MW wind turbine is compared over water depths of 10 to 50 meters. The comparison for different water depths can be seen in Table 5.1 where the calculated simulation is performed through an MCS with a sample size of 1000. The corresponding range given is for the mean of the 95% confidence interval.

Table 5.1: Comparison between foundation mass from literature and from calculation for a 5MW turbine

Waterdepth [m]	Mass literature [t]	Mass calculated [t]	Difference [%]
10	300	342 - 346	+14 - +15
12	390	382 - 385	-2.0 - -1.28
24	600	632 - 636	+5.3 - +6.0
40	1000	994 - 1001	-0.6 - +0.1
50	1200	687 - 733	-42 - -39

From this comparison, it can be said the preliminary design method can be used for smaller turbines for a range of 10 - 40 meters of water depth. Here the differences are minor and usually on the conservative side. After this range, the differences are too large and a trustworthy solution is less likely.

5.2.2. array cable length

As discussed in subsection 4.3.4 the total array cable length can be found through an internal cable optimization tool and the fast K-means preliminary cable routing calculation. These are both calculated through the individual turbine locations in the wind farm, the turbine-rated power, and the array cable-rated power. These inputs are fed into the model for an existing TotalEnergies wind farm and compared to the actual array cable length. The normalized array cable length can be found in Table 5.2 for the actual cable length, the found optimized cable length, and the fast preliminary cable routing calculation.

Table 5.2: Comparison between normalized real and calculated array cable length

Cable calculation	Normalized length [-]	Computing time [s]
Real cable	1.0	-
Optimized cable	1.20	7500
Preliminary cable	1.74	0.1

The user can define which cable calculation method should be used. For wind farms with a low amount of turbines, the optimization can be used for better results. In the case of a large amount of turbines, it is recommended to use the preliminary cable calculation to minimize computing time. With this being said, the user should be aware of the large overestimation of the cable length in the model when using the K-means method.

5.3. Fatigue behaviour

5.3.1. Fatigue lifetime

For fatigue, a comparison is made between the fatigue calculation outcome of an existing wind turbine in a TotalEnergies wind farm and the outcome of the fatigue calculated by the OpenFast Kriging surrogate model. The outcome of the fatigue calculation for the real case is that the turbine lifetime fatigue will stay under 0.33 [-], which corresponds with the safety factor of 3 which is commonly used as an industry standard for lifetime fatigue in wind turbines (TotalEnergies R&D internal, 2024). For the calculation through the surrogate model, the wind turbulence is calculated such that it takes into account the inter-turbine spacing of the existing wind farm. The most critical environmental conditions are selected, which are found by calculating the maximum values in the openFAST output. These can be found in Table 5.3

From this calculation, the lifetime fatigue is found to be significantly smaller than 0.33, thus verifying the calculation.

5.4. Vessel use

5.4.1. Construction time

To verify the construction time of the vessel use, the calculated prediction is compared with the actual project construction time. In section 4.5 the method for setting up standardized linear planning for

Table 5.3: Environmental conditions for maximum fatigue

Environmental condition	Value
Windspeed hub [m/s]	25
Wind heading [°]	0
Significant wave height [m]	11
wave period [s]	6
wave heading [°]	-90

offshore wind farm construction, maintenance, and decommissioning is explained. This linear planning calculation takes the user-defined stochastic activity durations as input. To verify, the parametric vessel use is calculated by using the turbine locations, types, and offshore locations of an existing TotalEnergies wind farm. From this wind farm, it is known that the construction was two years and the decommissioning is planned for one year. The exact amount of vessels used was not retrievable since this was executed by a sub-contractor. For this reason, it was chosen to use the activity durations as found in the literature with a minimum duration of being 25% earlier and a maximum duration of 50% later than the most likely duration. With these durations, the model also predicts a construction duration of 2 years and a decommissioning duration of 1 year. It is difficult to compare the maintenance duration since the wind farm is at the beginning of its lifetime and no data regarding this topic has been made available. However, it is assumed to be accurate since the construction and decommissioning are calculated according to the same method from the literature and are accurate.

5.5. Conclusion

From these analyses with reference cases from the literature and an actual TotalEnergies wind farm, the model is successfully verified with the limitations and application ranges taken into account.

6 Results

6.1. Introduction

Two main cases are going to be investigated to create results with the created model. The first case has the main goal of showing the IMAP-WFO's capability to compete with existing optimization models by finding the design that creates the minimum LCOE for a reference wind farm location and constraints. This confirms the applicability of the IMAP-WFO methodology and comments on the different user inputs necessary to find this minimum LCOE. The goal of the second case is to prove the added value of the proposed optimization framework by illustrating the versatility of the application the model can handle. The second case truly shows the broad application range of the IMAP-WFO methodology. Here, through the help of the preference functions, the control spectrum of an existing wind farm will be explored by varying the price of electricity and minimizing fatigue. Through this, the wind farm control with minimum fatigue for different price scenarios can be found.

6.2. Standard model settings

For the results, the settings of the model are summarized in Table 6.1

Table 6.1: Used standard setting to create results model

Setting	Used option
Cable current [A]	800
Friction angle [°]	30
Water depth [m]	50
Array cable voltage [kV]	66
Export cable voltage [kV]	132
Lifetime [years]	25
Sustainability scale [-]	ReCiPe human health
N Monte Carlo [-]	10
Material prices/day rates [euro]	Table D.1
Tower and monopile dimensioning method	Surrogate
Array cable calculation	K-means
GA population [-]	100
GA convergence criteria	subsubsection 2.1.5.2

Because of the high convergence criteria, the GA will need to reach multiple iterations where the same variant is deemed the optimum while 99 other variants are created. Through this high stall criteria, it is more likely to find a global instead of a local optimum since the solution space is actively investigated even when a variant has already proven itself as an optimum for multiple iterations.

6.3. Location cases

Both cases will be set up following the boundary conditions of an existing TotalEnergies wind farm in the North Sea, with typical environmental conditions and water depth. Due to confidentiality specifics can not be disclosed.

6.4. Case 1: minimum LCOE

6.4.1. Model set-up

The minimum LCOE case is the classical optimization application for wind farm design. It incorporates the minimization of all the costs while simultaneously maximizing the production, as can be seen in Equation 2.6. Within the created IMAP framework, this optimization is achieved by creating additional LCOE objective functions that can be minimized. The LCOE is calculated according to Equation 6.1 where the FCR is set to $1/T_{lifetime}$ which ensures a break-even LCOE at the end of a lifetime. This means that every year, an equal part of the CAPEX needs to be earned back such that after the lifetime, the whole CAPEX is earned back and break-even is reached In reality, a higher FCR will be chosen to increase profitability. This higher FCR is usually dependent on the investment strategy of which the wind farm is a part.

$$\text{LCOE} = \frac{(\text{CAPEX} * \text{FCR}) + (\text{OPEX} * T_{lifetime})}{\text{AEP} * T_{lifetime}} \tag{6.1}$$

With this new objective function, an optimization can be performed for just the LCOE when this objective is given the weight of 1. The preference function has 100 preference at an LCOE of 0 euros and 0 preference at an LCOE of 250 euros/MWh (the assumed maximum bound). These adjustments adapt the MODO model into a traditional SODO model that minimizes LCOE, for which reference research can be found in chapter 3. The design variable bounds for diameter follow the whole 3 to 30 MW interval possible through the surrogate model. For spacing, the range of 6 to 13 has been chosen based on industry standards (TotalEnergies R&D internal, 2024). The range of fleet size has been chosen between 1 and 10 since this gives a broad solution space. These design variable ranges can be found in Table 6.2.

Table 6.2: Bounds design variables minimization LCOE

Design variable	Lower bound	Upper bound
Turbine spacing [Turbine diameters]	6	13
Rotor diameter [m]	90	340
fleet size [-]	1	10

6.4.2. Optimization outcome

The minimized LCOE comes down to 18.78 euro/MWh, for an amount of 51 turbines with a diameter of 281 meters, individual spacing of 8.8 diameters, and 3 fleets for construction. Important to note is that none of the design variables went to the extreme values, but all converged to their optimum point within their ranges. This confirms this optimum since the solution space has been well identified. The optimal solution corresponds to a 20-22 MW turbine. This LCOE is lower than the interval found in [1] for offshore wind energy in 2023. Figure 6.1 shows the layout of this optimized wind farm and Figure 6.2 shows the individual preference functions in blue for the AEP, CAPEX, and OPEX objectives with the optimized outcome indicated as the black dot for each preference function.

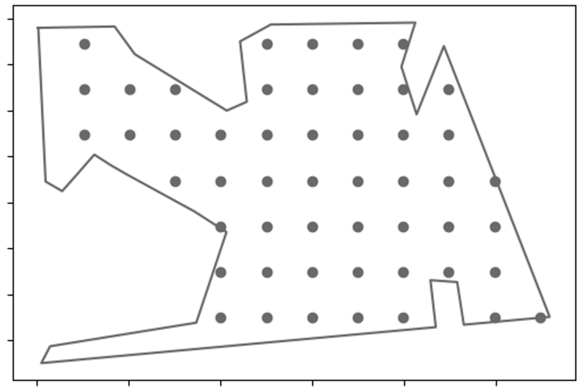

Figure 6.1: Optimized wind farm mayout

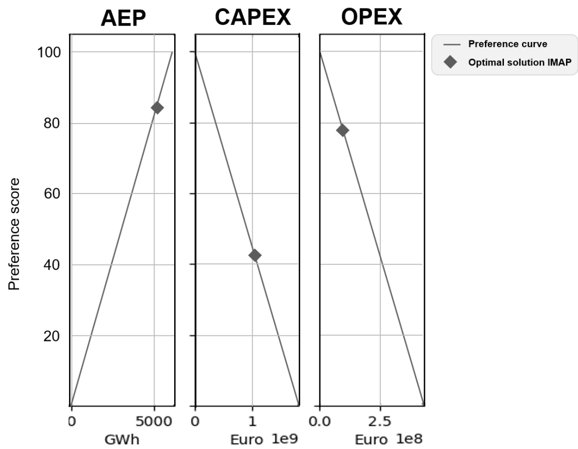

Figure 6.2: Preference functions and outcomes for minimized LCOE

These three economic drives for wind farms combine into the LCOE and their impact on this metric can give new insight into how to design future wind farms. In the preference functions, it can be seen that AEP has a high individual preference score of 84. CAPEX has a lower preference score of 42 and OPEX again has a high individual score of 78. The maximum x-value of these objectives represents the maximum value possible for these objectives within these ranges of design variables from Table 6.2. Within these ranges, AEP has a preference of 84 when compared to all the other AEP variants. From this, the individual weights of AEP, CAPEX, and OPEX can be calculated to be 0.41, 0.21, and 0.38 respectively by normalizing the preference scores. This shows the influence of these three objectives on the minimized LCOE through an IMAP approach.

6.5. Case 2: wind farm control

6.5.1. Model set-up

Wind farms can be controlled to produce a certain amount of energy per year to cover the operational expenditures and assure a certain return on initial investment, but with minimum overproduction. In this case study, such a controlling study will be performed through the IMAP-WFO framework. It will be investigated how many turbines of an existing wind farm should be used for production to find the amount of energy that is desired, while at the same time minimizing turbine tower lifetime fatigue due to bending moments for energy prices between 50 and 250 euro/MWh. To achieve this, first, the model outcome for CAPEX and OPEX need to be found for this existing wind farm. This is done by setting the design variables to the values of the actual wind farm. This gives the AEP, CAPEX, OPEX, and LCOE of the real wind farm, of which the CAPEX and OPEX will be used. With this CAPEX and OPEX, the rotor diameter is fixed in the model to represent the value of the turbines of the existing wind farm, but the inter-turbine spacing is made parametric. Because of this, the spacing can become larger than the original, which places fewer turbines in the same area, giving the total amount of turbines that should be turned on for a certain energy price. Since the turbines are placed in a grid, it can be identified which turbines disappear and thus can be turned off.

To couple the energy price to the optimization process, Equation 6.2 is used which gives the AEP based on CAPEX, yearly return on initial investment, OPEX, and energy price. For this indicative case, it is chosen that the yearly return on investment is again the breakeven point in the lifespan, which is $1/T_{lifetime}$%. In reality, this ROI will usually be chosen as a higher value to increase profitability. In this case, a certain contractual minimum energy delivery is not taken into account. It is assumed that only the energy price determines the amount of production.

$$\text{AEP} = \frac{(\text{CAPEX} * \text{ROI}) + \text{OPEX}}{\text{LCOE (energy price)}} \tag{6.2}$$

This AEP value can then be implemented in the optimization as a soft, steering constraint in the form of a triangular function for the preference function, as illustrated in Figure 6.3. This function has the desired AEP as a 100 score and then sharply decreasing scores for a lower and upper bound AEP. These bounds are still defined since they give the optimization algorithm the chance to improve on these bounds. This means that the optimization algorithm is told how to improve its next generation as long as a population member falls on the curve itself. If a signal function is used, the optimization algorithm would not be able to improve if the population does not contain the exact value on the first try. To make sure the optimization algorithm finds the values on this preference curve, the GA population should be sufficient and the bounds of the triangular distribution should be wide enough. This is achieved by setting the population to 100 and the bounds to 100.

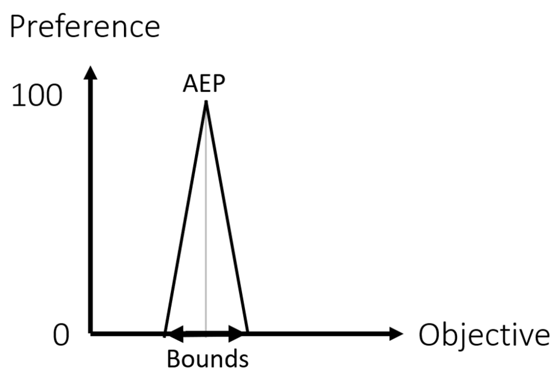

Figure 6.3: AEP preference function

6.5.2. Optimization outcome

The optimization has been performed for seven different energy prices between 50-250 euros/MWh. With this and the CAPEX and OPEX of the existing wind farm, the AEP for the desired energy price can be calculated. This AEP is put into the optimization model, from which a new wind farm is found. By comparing this new wind farm with the existing one, it can be deduced how many and which turbines should be used for production to guarantee a certain economical break-even production, while at the same time minimizing the fatigue loading on a farm scale. The amount of turbines that should be used for production can be seen in Table 6.3.

Table 6.3: wind farm control results

Energy price (euro/MWh)	wind farm AEP (MWh)	Producing turbines [-]
50	5493	114
75	3669	85
100	2754	64
125	2204	51
150	1838	42
200	1379	33
250	1103	25

An interesting result is that for the first 25-euro increase, only 75% of the turbines are still needed for break-even production. After the next 25-euro price increase, 75% of the remaining turbines and 56% of the turbines at 50 euro/MWh are still needed for energy production to maintain the break-even point. This trend changes at 125 euro, here 80% of the remaining turbines and 45% of the original turbines are needed for break-even energy production. At 150 euro/MWh 82% of the remaining turbines and 37% of the total turbines are needed for production. This is 79% and 29% for 200 euro/MWh and 76 and 22% for 250 euro/MWh. This behavior can be seen in Table 6.4 and Figure 6.4. From these, it becomes apparent that the largest change in needed turbines for production happens when going from 50 euro/MWh to 75 euro/MWh. After this, the percentage of turbines that can be turned off compared to the last price increase stays almost constant.

Table 6.4: Turbine operation by energy price table

Energy price (euro/MWh)	Turbines change local [%]	Turbines change global [%]
50	100	100
75	75	75
100	75	56
125	80	45
150	82	37
200	79	29
250	76	22

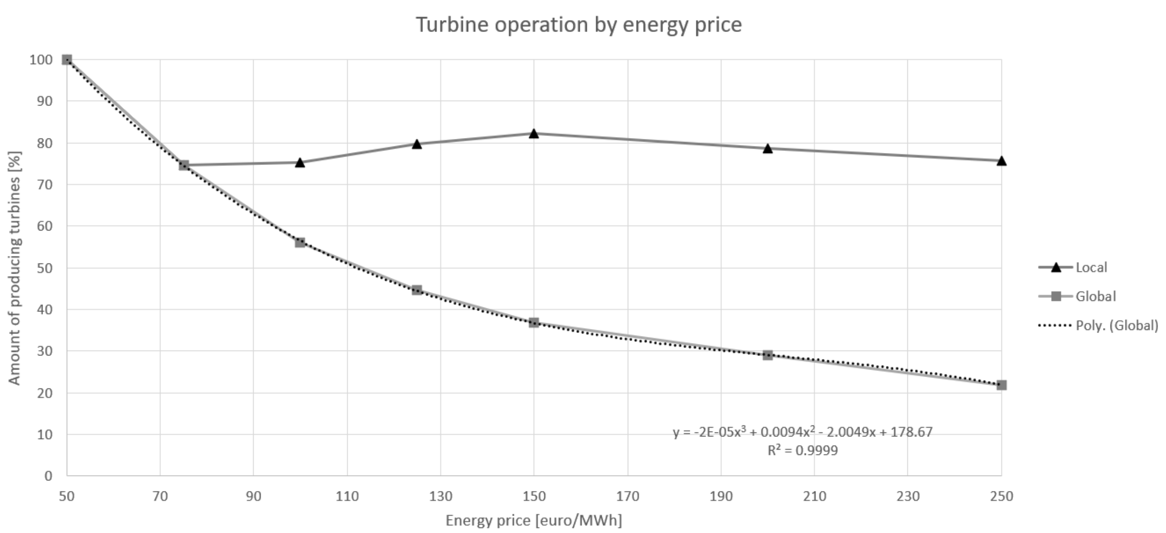

Figure 6.4: Turbine operation by energy price graph

From Figure 6.4, it can be seen that the largest difference in producing turbines for the wind farm control takes place in the price raise from 50 to 75 euro/MWh. However, the total amount of turbines follows the fitted polynomial curve that decreases to just 22 turbines producing at 250 euro/MWh. Figure 6.5 gives the control scheme for a reference wind farm. Here, grey shows producing, and black shows non-producing wind turbines over the different energy price scenarios.

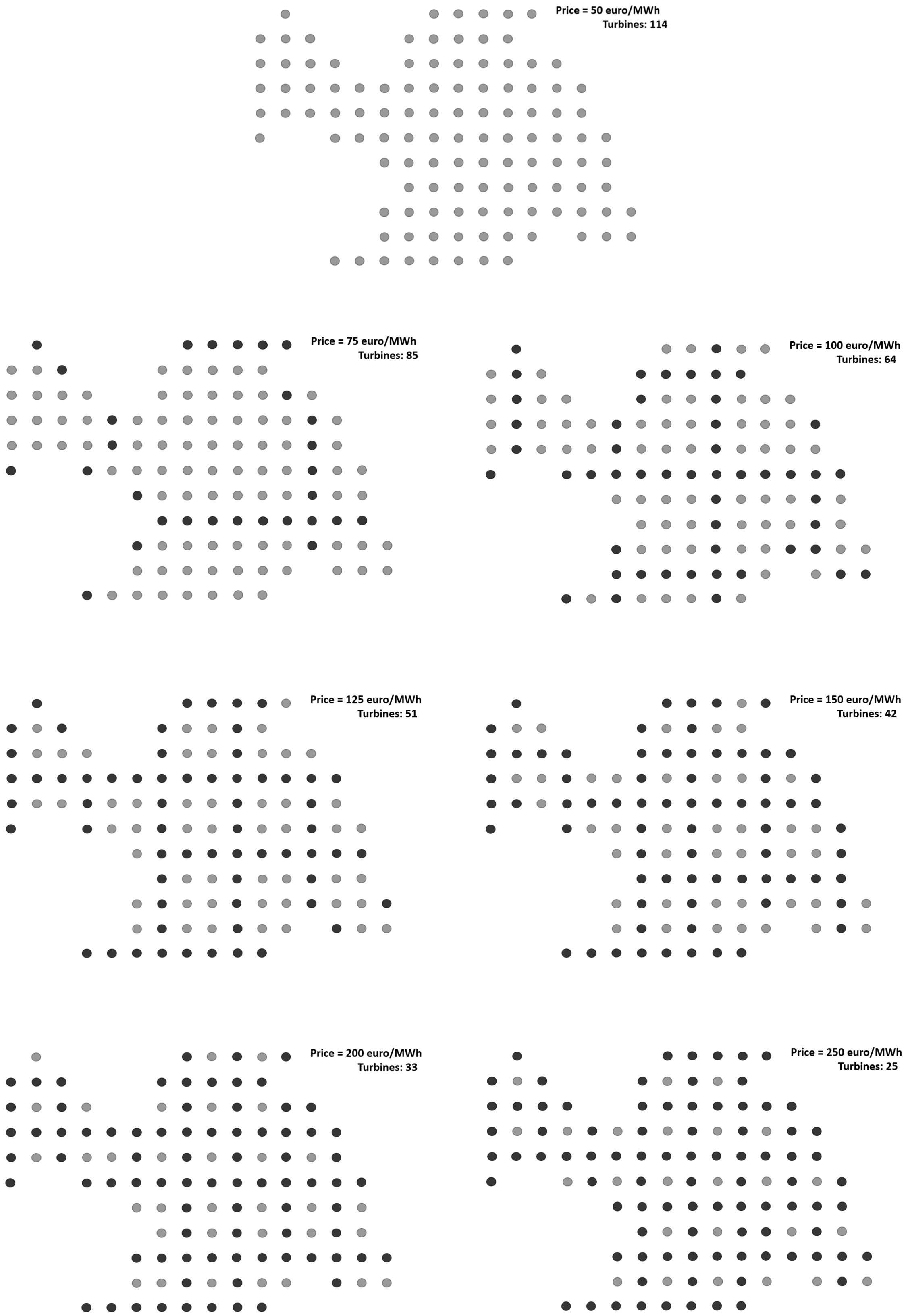

Figure 6.5: Wind farm control scheme for different energy prices where green shows the producing and red the non-producing turbines

7

Discussion & Conclusion

In this chapter, the results are interpreted and discussed, conclusions are drawn and perspective is provided.

7.1. Thesis summary

This thesis focuses on the optimization of offshore wind farms. Through the literature review, the most relevant optimization studies have been identified and analyzed, where the current state-of-the-art is inventoried. However, these optimization approaches lack the flexibility to be usable for multiple optimization tasks, have a low level of uncertainty quantification, and lack high-accuracy multi-physical behavior modeling. To fill this gap, a probabilistic IMAP optimization approach (IMAP-WFO) is constructed with the help of Kriging meta-models.

This is done by creating parametric design performance functions that model the physical behavior of a wind farm. These are parametric energy production, material use, vessel use, and fatigue. All of these, except the vessel use, are constructed based on Kriging meta-models and are all simulated through Monte Carlo simulations to quantify the uncertainty.

These design performance functions are successfully verified by comparison with an existing wind farm where the model outcomes are compared to reality. This not only verifies the design performance functions but also identifies the model limitations.

These technical functions are translated to the desired socio-economic behavior in the objective functions. The created objective functions represent the wind farm's sustainability based on nine usable sustainability scales, the Annual Energy Production, the Capital Expenditure, the Operational Expenditure, the lifetime fatigue, and the meta-model uncertainty. These objectives can be toggled on and off through the user-defined weights, which enables flexible optimization purposes. Also, the users' desired outcomes on these objectives are translated through the preference functions.

With this completed model, two result cases are realized. The goal of the first case is to convey the model's capability to compete with existing models. This case follows the classic optimization goal found in literature, the minimization of the LCOE. As a result of this case, an LCOE of 18.78 euros is found for a wind farm with 51 281-meter diameter turbines with an individual spacing of 8.8 diameters and a standardized construction fleet size of 3. The goal of the second case is to prove the added value of the proposed optimization framework by illustrating the versatility in the application that the model can handle. This case optimizes the wind farm control and investigates the strategy for certain energy prices while minimizing the turbine lifetime fatigue. From this, a control strategy is found for a reference wind farm for energy prices from 50-250 euro/MWh.

7.2. Discussion

From the first result case, it has been shown that the optimal wind farm, based on the boundary conditions, is composed of 51 turbines with a diameter of 281 meters, an inter-turbine spacing of 8.8, and a standardized construction fleet size of 3. This corresponds to a wind farm using 20-22MW turbines and gives an LCOE of 18.78 euros/MWh. These 20-22MW turbines are on the industry roadmap to be developed in the coming years. This means that minimal LCOE is found by using larger turbines than the ones used nowadays. However, it also implies that larger turbines are not necessarily more profitable since the optimization converged towards a diameter of 281 meters instead of the limit of 340 meters. The LCOE is lower than found in literature or reference projects and is thus a surprising result. Logically, the LCOE is quite low since the model converged to a turbine size that is not yet feasible in the present. The model does not take supply chain and construction issues into account, which for these very large wind turbines, can be problematic for their realization Tijdeman et al. [42].

From the minimized LCOE, the individual contributions from AEP, CAPEX, and OPEX can be found through their preference scores. When calculated, the individual weights are 0.41, 0.38, and 0.21 for AEP, OPEX, and CAPEX respectively. This indicates that the production of AEP has the largest influence. Second is OPEX and third is CAPEX. This result can be explained by how the LCOE is calculated with the fixed charge rate. The FCR is chosen to reach a break-even point after the full lifetime. For this reason, CAPEX has a decreased influence on the LCOE. In this light, these results make sense since an increase in AEP will make the largest decrease in LCOE possible. If a larger FCR was chosen, CAPEX would have a higher significance compared to the AEP and OPEX and would shift in importance. The importance of the individual weight of CAPEX is thus dependent on the FCR, which determines the profitability of the wind farm. With a higher FCR, the relative contribution of OPEX would go down while the contribution of CAPEX would go up. The identification of these exact weights for different FCRs can be valuable for future investment and design decisions.

The second result case investigated the operation optimization. For different energy prices, the operation was optimized by minimizing the lifetime fatigue of the wind turbines. From this, it was found how many and which turbines should be used for production for certain energy prices to minimize fatigue behavior. This is a valuable result that can significantly prolong the lifetime of wind turbines in the wind farm and decrease the operational expenses, thus decreasing the LCOE. If wind turbines can be taken out of the producing state by feathering the blades, this will decrease the loading and fatigue. When the loading decreases, the fatigue lifetime increases. Through a longer producing lifetime, the LCOE will decrease since the CAPEX, normally spread over the nominal lifetime, is now spread over an extended lifetime. This gives a higher margin for profitability.

Besides, it is found where the largest difference in wind farm operation takes place. This is from 50 to 75 euro/MWh, where 25% of the turbines can be taken out of production. At the maximum energy price bound of 250 euro/MWh, 78% of the turbines can be taken out of production, showing a significant impact on the control possibilities.

However, the scenario where the control is completely dependent on the energy price is a simplification of reality. In reality, the energy producer would have agreements with clients about a certain minimal production. This production would need to be guaranteed, meaning that the proposed control scenario is not applicable until this minimal production is met. Everything above this minimum could be controlled in the described manner.
Also, the control scheme prescribes a static measure for a certain energy price. If the energy price stays steady for an extended period, this will thus load the turbines that are active for this control scheme. In this case, a more adaptive strategy would need to take place to keep decreasing fatigue for these turbines.

Another limitation for both case studies is that the optimization has only been performed with the settings as described in section 6.2. Eventhough the population size and stall criteria have been chosen high enough to make sure the solution space is thoroughly investigated, different populations sizes and stall criteria have not been investigated. This means that the minimum value for these two settings where the model still finds the global optimum has not been identified.

These results validate the application of the optimization framework within offshore wind farm design optimization and serve as a proof of concept for the methodology.

7.3. Conclusion

This study focuses on the parametric optimization of wind farm design. It has the goal of creating a flexible and accurate optimization tool to answer the following research question:

How is the Levelized Cost of Energy (LCOE) influenced by employing a probabilistic multi-objective strategy based Integrative Maximised Aggregated Preference (IMAP) optimization approach in the design of offshore wind farms?

To answer this research question, first, the supporting research questions need to be answered.

The key design variables optimizable in offshore wind farm design are rotor diameter, inter-turbine spacing, and the construction fleet size. These variables significantly impact the cost and production characteristics of such wind farms. The energy production is established through an analytical model and a Kriging meta-model. The material use is calculated through a Kriging meta-model and trends from the literature. The vessel use is determined through parametric network planning and standardized vessel durations from the literature. The fatigue behavior of a parametric wind farm can be determined from a Kriging meta-model created from a surrogate model from openFAST. From these variables and models, the sustainability, Annual Energy Production (AEP), Capital Expenditure (CAPEX), Operational Expenditure (OPEX), lifetime fatigue, and model uncertainty objectives can be determined and optimized. This approach allows for a quantitative expression of the impacts of the key design variables on the performance and cost-effectiveness of offshore wind farms.

The primary method to capture and quantify the strategy of the operator in the layout design of offshore wind farms is by identifying the contributions of AEP, CAPEX, and OPEX to the LCOE for a certain fixed charge rate. For wind farm operations, the strategy can be quantified by the market energy price. This strategy allows wind turbines to be taken out of production to minimize fatigue while maintaining a set production revenue. These approaches integrates the operator's strategy into the characteristics of an offshore wind farm, guiding decision-making processes.

The developed model can be effectively verified by comparing its output to an existing TotalEnergies wind farm under the same boundary conditions and cases from the literature. These comparisons verified the model by giving similar results, while simultaneously revealing certain limitations in the model, such as the overestimation of array-cable length and a minor underestimation of energy production. These limitations should be taken into account by the model user. Evidence of the reduction in LCOE achievable through the proposed probabilistic strategy-based IMAP optimization approach in wind farm design is obtained by using the model to minimize the LCOE and comparing the outcome to reference values from the literature. This comparison demonstrates the reduction in LCOE.

This brings us back to the main research question. It can be concluded that the proposed optimization framework can find an optimal wind farm design by applying a standard wind farm design optimization method through the minimization of the LCOE. With the found LCOE of 18.83 euros/MWh, this shows a sharp decrease compared to references from literature and reference projects. The optimized wind farm consists of wind turbines in the 20-22 MW range, which is on the current development roadmap for the offshore wind industry.

Besides, the individual contributions of the AEP, CAPEX, and OPEX to the LCOE can be identified for this optimized wind farm for an FCR that represents financial break-even at the end-of-life of the wind farm. These are important indicators that can be used in strategic investment and design decisions. These individual weights display the power of the proposed optimization framework to optimize for a global performance indicator such as LCOE or for the AEP, CAPEX, and OPEX, which are the contributors to this.

Next to this, it can also be concluded that the proposed optimization framework can influence the LCOE through the optimization of operations under different energy prices. It has been shown that by minimizing wind turbine fatigue while fixing the production corresponding to a certain energy price, not all turbines need to be used for production. The ability to know how many and which of these turbines can be taken out of production allows the operator to minimize the fatigue loads on these turbines, giving them a longer service life. Through this longer service life, the LCOE will be decreased since the same initial investment can be spread over a longer operation service life than initially assumed.

Besides this operation advice, it is also identified where the sharpest decrease in production can take place. This is from 50 to 75 euros/MWh, where approximately 25% of the turbines can be taken out of production to minimize fatigue. At the energy price bound of 250 euro/MWh, 78% of the turbines that were producing at 50 euro/MWh can be taken out of production.

All this considered, it can be concluded that the proposed framework positively influences the LCOE in the two investigated cases. In both the case of the wind farm design optimization and the wind farm operation optimization, the LCOE is or can be lowered when compared to the reference or standard methods. This shows the main advantage of the proposed framework. Instead of just minimizing the LCOE, which is a static cost indicator looking into the profitability of a wind farm, the framework can also be used in the more adaptive problems that come into play with renewable energy sources where energy generation can fluctuate. Because of the non-linear optimization character of the framework, the wind farm operation can be optimized; retaining a set income, while minimizing the fatigue loading behavior. This can result in adaptive wind farm control based on the energy price. Through this, a longer service lifetime can be achieved, which will greatly decrease the LCOE.

7.4. Impact

The optimization of wind farm design, as explored in this thesis, has significant societal implications. By improving the efficiency and reducing the LCOE for offshore wind farms, this research contributes to the broader goal of transitioning to renewable energy sources. This transition is critical for addressing climate change, reducing greenhouse gas emissions, and enhancing energy security.

Furthermore, the integration of advanced optimization techniques and probabilistic design methods can lead to more reliable and cost-effective wind energy solutions. This can result in lower energy costs for consumers and greater economic viability for wind energy projects, potentially leading to increased investment in renewable energy infrastructure.

Moreover, the adoption of cleaner energy sources can have positive health impacts by reducing air pollution associated with fossil fuel-based power generation. This can lead to improved public health outcomes and reduced healthcare costs.

In summary, the advancements in wind farm design optimization presented in this thesis not only contribute to the technical and economic aspects of renewable energy but also have profound societal benefits, aligning with global sustainability goals and enhancing the quality of life for communities.

7.5. Perspective

Looking back at this thesis, some potential future research possibilities are presented here. These perspectives are organized into model improvements and follow-up studies.

7.5.1. Model improvements

Due to limited time and computational power, the model has been simplified in some manners to be able to create results. Possible improvements that can be made given increased resources are:

- **Array cable length**: In the current model, it was computationally too expensive to run an array cable optimizer, even though it has been shown to create better results. If given better computational resources or with an improved Capacitated Minimal Spanning Tree model, a higher level of accuracy could be achieved.
- **Fatigue surrogate**: Due to time restrictions, limited access to available HPC resources, and HPC maintenance during the project, it was only possible to include one turbine diameter to the fatigue surrogate model instead of the initially conceived 3 to 5. Adding more turbine diameters will increase the accuracy of the fatigue behavior in the model.
- **Monte Carlo simulations**: Due to the computational limitations, it was only possible to create the results through Monte Carlo simulations with a sample size of 10. This is due to a shortage of memory on the computer for a larger sample size. Even though the lower number of simulations gives a larger uncertainty spread, it is still deemed more accurate compared to deterministic values, since more information about the possible error is available. However, with more computational resources available, it is advised to have a larger sample size to increase accuracy.
- **Kriging meta-model**: To increase the accuracy of the Kriging meta-model, finding additional surrogate points that have the highest effect in increasing the model accuracy should be adapted. By finding the standard deviation for all the points in between the defined discrete surrogate points, it can be found where the standard deviation is the highest. To increase meta-model accuracy through additional surrogate points, it is advised to prioritize these points with high standard deviation to mitigate as much inaccuracy as possible.

7.5.2. Follow up studies

With this methodology, some interesting additional possible studies came to light during this thesis. These are the following.

- **Find AEP, CAPEX, and OPEX contributions to LCOE for different FCRs**: In this study, the influence of AEP, CAPEX, and OPEX on LCOE for an optimized wind farm has been investigated for the FCR that represents the break-even after full lifetime. However, FCR usually represents a certain strategic profit profile that was decided upon during the investment decision. An interesting study would be to see what the contributions of AEP, CAPEX, and OPEX are on LCOE for increasingly profitable FCR rates. This could give a major advantage for investment and design decision-making.
- **Exact decrease in fatigue due to control optimization**: This research has presented the proof of concept for control optimization. Fatigue is minimized for a certain production to find the necessary producing turbines. However, how much fatigue is mitigated through this strategy, and how much additional service lifetime can be achieved through this are questions that still need answering. Through a follow-up study, a quantifiable number can be identified for the advantage of the control optimization.
- **Include power purchase agreements with wind farm optimization control**: In this study, it is assumed that wind farm operation is only influenced by the energy price. In reality, there is often a minimum production that is agreed upon in a power purchase agreement (PPA). Everything that is produced above the minimum that needs to be delivered can still be optimized through control optimization. A follow-up study can result in a more realistic application range for control optimization.

- **Flexible wind farm control**: Instead of turning turbines on or off to control the wind farm, a flexible approach can also be used through wake steering. Here, a turbine can be misaligned with the wind to a certain degree to enable more airflow through the wind farm. However, this will increase the fatigue loads on these turbines as well. Finding an optimum in this might prove useful.
- **Sensitivity analysis GA settings**: Re-running the same case for different population sizes and N-stall criteria to check what the minimum values are for this problem where the GA still finds the global optimum.

Bibliography

[1] *2023 Levelized Cost Of Energy+*. https://www.lazard.com. URL: https://www.lazard.com/research-insights/2023-levelized-cost-of-energyplus/ (visited on 05/29/2024).

[2] Ahmed A. AbdulHamed, Medhat A. Tawfeek, and Arabi E. Keshk. "A genetic algorithm for service flow management with budget constraint in heterogeneous computing". In: *Future Computing and Informatics Journal* 3.2 (2018), pp. 341–347. ISSN: 2314-7288. DOI: https://doi.org/10.1016/j.fcij.2018.10.004. URL: https://www.sciencedirect.com/science/article/pii/S2314728818300370.

[3] Evgeny Atlaskin, Irene Suomi, and Anders Lindfors. "Statistical calculation of thrust curve of a wind turbine based on available power curve and general specifications data". In: (Apr. 1, 2021). Conference Name: EGU General Assembly Conference Abstracts ADS Bibcode: 2021EGUGA..2314402A, EGU21–14402. DOI: 10.5194/egusphere-egu21-14402. URL: https://ui.adsabs.harvard.edu/abs/2021EGUGA..2314402A (visited on 06/14/2024).

[4] S. Bhat and R. Patibandl. "Metal Fatigue and Basic Theoretical Models: A Review". In: *Alloy Steel - Properties and Use*. Ed. by Eduardo Valencia Morales. InTech, Dec. 22, 2011. ISBN: 978-953-307-484-9. DOI: 10.5772/28911. URL: http://www.intechopen.com/books/alloy-steel-properties-and-use/metal-fatigue-and-basic-theoretical-models-a-review (visited on 04/16/2024).

[5] Benjamin S. Blanchard and W. J. Fabrycky. *Systems engineering and analysis*. 5th ed. Prentice Hall international series in industrial and systems engineering. OCLC: ocn457159070. Boston: Prentice Hall, 2011. 786 pp. ISBN: 978-0-13-221735-4 978-0-13-196326-9.

[6] Peter Bonate. "A Brief Introduction to Monte Carlo Simulation". In: *Clinical pharmacokinetics* 40 (Feb. 1, 2001), pp. 15–22. DOI: 10.2165/00003088-200140010-00002.

[7] Vicki Buchan. "Offshore Substations: Fixed or Floating? – Technoeconomic Analysis". In: (2021).

[8] D.J.T. Carter. "Prediction of wave height and period for a constant wind velocity using the JONSWAP results". In: *Ocean Engineering* 9.1 (Jan. 1982), pp. 17–33. ISSN: 00298018. DOI: 10.1016/0029-8018(82)90042-7. URL: https://linkinghub.elsevier.com/retrieve/pii/0029801882900427 (visited on 06/03/2024).

[9] R. Damiani, K. Dykes, and G. Scott. "A comparison study of offshore wind support structures with monopiles and jackets for U.S. waters". In: *Journal of Physics: Conference Series* 753.9 (Sept. 2016). Publisher: IOP Publishing, p. 092003. ISSN: 1742-6596. DOI: 10.1088/1742-6596/753/9/092003. URL: https://dx.doi.org/10.1088/1742-6596/753/9/092003 (visited on 05/16/2024).

[10] *Data,Tools,Books*. Sustainability Impact Metrics. URL: https://www.ecocostsvalue.com/data-tools-books/ (visited on 04/17/2024).

[11] Katherine Dykes. "Optimization of Wind Farm Design for Objectives Beyond LCOE". In: *Journal of Physics: Conference Series* 1618.4 (Sept. 1, 2020), p. 042039. ISSN: 1742-6588, 1742-6596. DOI: 10.1088/1742-6596/1618/4/042039. URL: https://iopscience.iop.org/article/10.1088/1742-6596/1618/4/042039 (visited on 12/17/2023).

[12] Jan Emblemsvåg. "On the levelised cost of energy of windfarms". In: *International Journal of Sustainable Energy* 39.7 (Aug. 8, 2020). Publisher: Taylor & Francis _eprint: https://doi.org/10.1080/14786451.2020.17537 pp. 700–718. ISSN: 1478-6451. DOI: 10.1080/14786451.2020.1753742. URL: https://doi.org/10.1080/14786451.2020.1753742 (visited on 02/26/2024).

[13] E. Faraggiana et al. "An efficient optimisation tool for floating offshore wind support structures". In: *Energy Reports* 8 (Nov. 1, 2022), pp. 9104–9118. ISSN: 2352-4847. DOI: 10.1016/j.egyr.2022.07.036. URL: https://www.sciencedirect.com/science/article/pii/S2352484722013014 (visited on 06/03/2024).

[14] L. Fingersh, M. Hand, and A. Laxson. *Wind Turbine Design Cost and Scaling Model*. NREL/TP-500-40566. Dec. 1, 2006, NREL/TP–500–40566. DOI: 10.2172/897434. URL: http://www.osti.gov/servlets/purl/897434-Feoadi/ (visited on 04/16/2024).

[15] J. Serrano González et al. "Overall design optimization of wind farms". In: *Renewable Energy* 36.7 (July 2011), pp. 1973–1982. ISSN: 09601481. DOI: 10.1016/j.renene.2010.10.034. URL: https://linkinghub.elsevier.com/retrieve/pii/S0960148110005495 (visited on 12/28/2023).

[16] Yinghou He et al. "Spatiotemporal variation in air density and associated effects on the wind-induced response of high-rise buildings". In: *Engineering Structures* 264 (Aug. 1, 2022), p. 114428. ISSN: 0141-0296. DOI: 10.1016/j.engstruct.2022.114428. URL: https://www.sciencedirect.com/science/article/pii/S0141029622005399 (visited on 04/16/2024).

[17] Edwin Hernandez-Estrada et al. "Considerations for the structural analysis and design of wind turbine towers: A review". In: *Renewable and Sustainable Energy Reviews* 137 (Mar. 1, 2021), p. 110447. ISSN: 1364-0321. DOI: 10.1016/j.rser.2020.110447. URL: https://www.sciencedirect.com/science/article/pii/S1364032120307346 (visited on 03/04/2024).

[18] Harold van Heukelum et al. "Preference-based service life design of floating wind structures". In: June 28, 2023, pp. 957–964. ISBN: 978-1-00-332302-0. DOI: 10.1201/9781003323020-116.

[19] Quentin Huchet. "Kriging based methods for the structural damage assessment of offshore wind turbines". PhD thesis. Université Clermont Auvergne [2017-2020], Dec. 13, 2018. URL: https://theses.hal.science/tel-02130870 (visited on 04/19/2024).

[20] M A J Huijbregts et al. "© RIVM 2017 Parts of this publication may be reproduced, provided acknowledgement". In: (2016).

[21] Andrew Kusiak and Zhe Song. "Design of wind farm layout for maximum wind energy capture". In: *Renewable Energy* 35.3 (2010). Publisher: Elsevier, pp. 685–694. URL: https://ideas.repec.org//a/eee/renene/v35y2010i3p685-694.html (visited on 06/02/2024).

[22] Wing Yin Kwong et al. "Multi-Objective Wind Farm Layout Optimization Considering Energy Generation and Noise Propagation With NSGA-II". In: *Proc. International Design Engineering Technical Conferences & Computers and Information in Engineering Conference (IDETC/CIE'12)* 136 (Aug. 12, 2012), pp. 1–10. DOI: 10.1115/DETC2012-71478.

[23] Jani Laine et al. "Seminar on Case Studies in Operations Research Expert judgements for cost assessment in risk management Final Report". In: ().

[24] Markus Lerch, Mikel De-Prada-Gil, and Climent Molins. "Collection Grid Optimization of a Floating Offshore Wind Farm Using Particle Swarm Theory". In: *Journal of Physics: Conference Series* 1356 (Oct. 1, 2019), p. 012012. DOI: 10.1088/1742-6596/1356/1/012012.

[25] Chen Li et al. "Environmental Impacts of Global Offshore Wind Energy Development until 2040". In: *Environmental Science & Technology* 56.16 (Aug. 16, 2022). Publisher: American Chemical Society, pp. 11567–11577. ISSN: 0013-936X. DOI: 10.1021/acs.est.2c02183. URL: https://doi.org/10.1021/acs.est.2c02183 (visited on 03/26/2024).

[26] Chen Li et al. "Future material requirements for global sustainable offshore wind energy development". In: *Renewable and Sustainable Energy Reviews* 164 (Aug. 1, 2022), p. 112603. ISSN: 1364-0321. DOI: 10.1016/j.rser.2022.112603. URL: https://www.sciencedirect.com/science/article/pii/S1364032122004993 (visited on 03/27/2024).

[27] Mingxin Li et al. "A multi-objective maintenance strategy optimization framework for offshore wind farms considering uncertainty". In: *Applied Energy* 321 (Sept. 1, 2022), p. 119284. ISSN: 0306-2619. DOI: 10.1016/j.apenergy.2022.119284. URL: https://www.sciencedirect.com/science/article/pii/S0306261922006419 (visited on 03/05/2024).

[28] Paul A. Lynn. *Onshore and Offshore Wind Energy: An Introduction*. Google-Books-ID: 6CstrP_IXQ4C. John Wiley & Sons, Dec. 12, 2011. 237 pp. ISBN: 978-0-470-97608-1.

[29] Nina Morozova et al. “A CFD-based surrogate model for predicting flow parameters in a ventilated room using sensor readings”. In: *Energy and Buildings* 266 (July 2022), p. 112146. ISSN: 03787788. DOI: 10.1016/j.enbuild.2022.112146. URL: https://linkinghub.elsevier.com/retrieve/pii/S0378778822003176 (visited on 06/19/2024).

[30] Caitlin T. Mueller and John A. Ochsendorf. “Combining structural performance and designer preferences in evolutionary design space exploration”. In: *Automation in Construction* 52 (Apr. 2015), pp. 70–82. ISSN: 09265805. DOI: 10.1016/j.autcon.2015.02.011. URL: https://linkinghub.elsevier.com/retrieve/pii/S0926580515000308 (visited on 03/19/2024).

[31] M.M. Pedersen et al. *PyWake 2.5.0: An open-source wind farm simulation tool*. Feb. 2023. URL: https://gitlab.windenergy.dtu.dk/TOPFARM/PyWake.

[32] Alex Powell. *Intro to Gaussian Process Regression*. Medium. Jan. 10, 2021. URL: https://towardsdatascience.com/intro-to-gaussian-process-regression-14f7c647d74d (visited on 06/24/2024).

[33] Sohail Reddy. “Wind Farm Layout Optimization (WindFLO) : An advanced framework for fast wind farm analysis and optimization”. In: *Applied Energy* 269 (May 15, 2020). DOI: 10.1016/j.apenergy.2020.115090.

[34] S. Rodrigues, P. Bauer, and Peter A. N. Bosman. “Multi-objective optimization of wind farm layouts – Complexity, constraint handling and scalability”. In: *Renewable and Sustainable Energy Reviews* 65 (Nov. 1, 2016), pp. 587–609. ISSN: 1364-0321. DOI: 10.1016/j.rser.2016.07.021. URL: https://www.sciencedirect.com/science/article/pii/S1364032116303458 (visited on 12/28/2023).

[35] Yves-Marie Saint-Drenan et al. “A parametric model for wind turbine power curves incorporating environmental conditions”. In: *Renewable Energy* 157 (Sept. 1, 2020), pp. 754–768. ISSN: 0960-1481. DOI: 10.1016/j.renene.2020.04.123. URL: https://www.sciencedirect.com/science/article/pii/S0960148120306613 (visited on 02/27/2024).

[36] Mahmood Shafiee, Feargal Brennan, and Inés Armada Espinosa. “A parametric whole life cost model for offshore wind farms”. In: *The International Journal of Life Cycle Assessment* 21.7 (July 1, 2016), pp. 961–975. ISSN: 1614-7502. DOI: 10.1007/s11367-016-1075-z. URL: https://doi.org/10.1007/s11367-016-1075-z (visited on 04/08/2024).

[37] Kabir Bashir Shariff and Sylvain S. Guillou. “An empirical model accounting for added turbulence in the wake of a full-scale turbine in realistic tidal stream conditions”. In: *Applied Ocean Research* 128 (Nov. 1, 2022), p. 103329. ISSN: 0141-1187. DOI: 10.1016/j.apor.2022.103329. URL: https://www.sciencedirect.com/science/article/pii/S0141118722002619 (visited on 04/16/2024).

[38] Sami Yamani Douzi Sorkhabi et al. “Constrained Multi-Objective Wind Farm Layout Optimization: Introducing a Novel Constraint Handling Approach Based on Constraint Programming”. In: *Volume 2A: 41st Design Automation Conference*. ASME 2015 International Design Engineering Technical Conferences and Computers and Information in Engineering Conference. Boston, Massachusetts, USA: American Society of Mechanical Engineers, Aug. 2, 2015, V02AT03A031. ISBN: 978-0-7918-5707-6. DOI: 10.1115/DETC2015-47535. URL: https://asmedigitalcollection.asme.org/IDETC-CIE/proceedings/IDETC-CIE2015/57076/Boston,%20Massachusetts,%20USA/254346 (visited on 06/02/2024).

[39] Ishwarya Srikanth et al. “Simplified Design Procedure of Monopile Foundation for Offshore Wind Turbine in Gujarat, India”. In: *Journal of Shipping and Ocean Engineering* 7 (Aug. 28, 2017). DOI: 10.17265/2159-5879/2017.04.001.

[40] Herbert J. Sutherland. *On the Fatigue Analysis of Wind Turbines*. SAND99-0089. Sandia National Lab. (SNL-NM), Albuquerque, NM (United States); Sandia National Lab. (SNL-CA), Livermore, CA (United States), June 1, 1999. DOI: 10.2172/9460. URL: https://www.osti.gov/biblio/9460 (visited on 03/25/2024).

[41] Sheng-Lun Tai et al. *Validation of Turbulence Intensity as Simulated by the Weather Research and Forecasting Model off the U.S. Northeast Coast*. Oct. 10, 2022. DOI: 10.5194/wes-2022-84. URL: https://wes.copernicus.org/preprints/wes-2022-84/wes-2022-84.pdf (visited on 04/16/2024).

[42] Dimitri Tijdeman et al. “Comparative feasibility study of a 30 MW disruptive floater solution with a 15 MW PivotBuoy and a benchmark 15 MW semi-submersible floater in the Bay of Biscay”. In: (2023). URL: https://repository.tudelft.nl/islandora/object/uuid%3Afeb24818-1ef3-4db7-9547-5d9a709051a1 (visited on 06/06/2024).

[43] Raymond Tran et al. “Fast and effective multi-objective optimisation of wind turbine placement”. In: *Proceedings of the 15th annual conference on Genetic and evolutionary computation*. GECCO ’13. New York, NY, USA: Association for Computing Machinery, July 6, 2013, pp. 1381–1388. ISBN: 978-1-4503-1963-8. DOI: 10.1145/2463372.2463541. URL: https://doi.org/10.1145/2463372.2463541 (visited on 06/02/2024).

[44] Kalyan Veeramachaneni et al. “Optimizing energy output and layout costs for large wind farms using particle swarm optimization”. In: June 1, 2012, pp. 1–7. ISBN: 978-1-4673-1510-4. DOI: 10.1109/CEC.2012.6253002.

[45] J.A. Voormolen, H.M. Junginger, and W.G.J.H.M. Van Sark. “Unravelling historical cost developments of offshore wind energy in Europe”. In: *Energy Policy* 88 (Jan. 2016), pp. 435–444. ISSN: 03014215. DOI: 10.1016/j.enpol.2015.10.047. URL: https://linkinghub.elsevier.com/retrieve/pii/S0301421515301749 (visited on 12/10/2023).

[46] Piotr Wais. “A review of Weibull functions in wind sector”. In: *Renewable and Sustainable Energy Reviews* 70 (C 2017). Publisher: Elsevier, pp. 1099–1107. ISSN: 1364-0321. URL: https://econpapers.repec.org/article/eeerensus/v_3a70_3ay_3a2017_3ai_3ac_3ap_3a1099-1107.htm (visited on 06/03/2024).

[47] Longyan Wang, Andy Tan, and Yuantong Gu. “A novel control strategy approach to optimally design a wind farm layout”. In: *Renewable Energy* 95 (Sept. 2016), pp. 10–21. ISSN: 09601481. DOI: 10.1016/j.renene.2016.03.104. URL: https://linkinghub.elsevier.com/retrieve/pii/S0960148116302889 (visited on 12/28/2023).

A

Appendix A: PyWake wakemodels

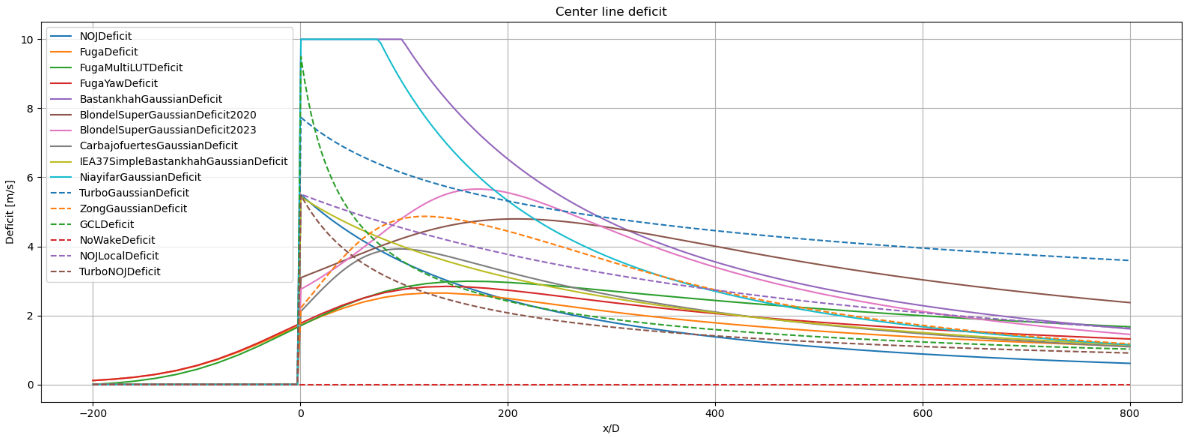

Figure A.1: Deficit along center line from different models, [31].

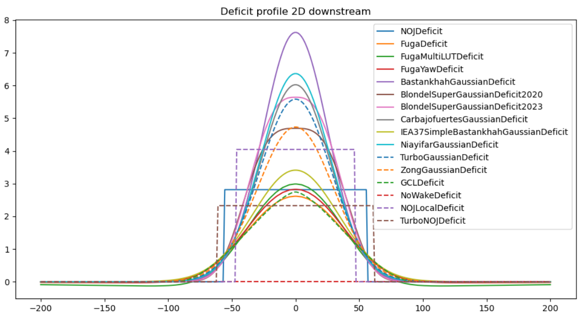

Figure A.2: 2 diameter spacing deficit profile, [31].

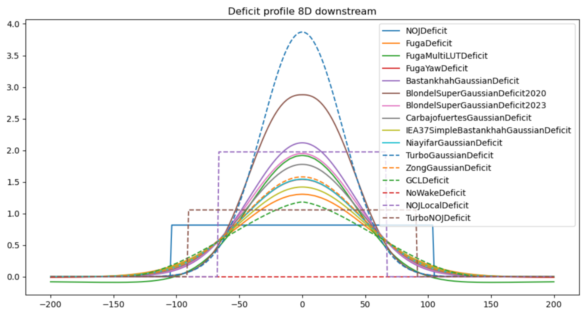

Figure A.3: 8 diameter spacing deficit profile, [31].

B

Appendix B: Standardized vessel use

For vessel use, a lifecycle analysis (LCA) will be used to identify the specific activities and resources necessary for the construction, maintenance, and decommissioning of wind farms. These activities and resources are gathered and quantified for general wind farms by [25], which is assumed to be valid for the possible wind farm configurations in this thesis.

B.0.0.1 Construction

The construction phase consists of three main construction processes. These are the installation of foundations, turbines, and array cables. During the installation of foundations, the necessary equipment and materials are towed from shore to the production location. Here the foundation is installed and afterwards grouted in place. Finally, rock is dumped as scour protection. This process is further described in Table B.1. The work times are listed as hours per turbine.

Table B.1: Foundation construction cycle

Activity	Equipment	Amount of equipment	Work time [h/turbine]
Foundation transport	Tugboat	2	10.27
Transport of jack-up	Tugboat	2	3.6
Construction of foundation	Jack-up	1	24
Transportation of pump	Barge	1	24
Injection of grout	Barge	1	24
Transportation of rock	Barge	1	5.13
Dumping of rock	Barge	1	29

For the installation of the turbine, a jack-up barge needs to be moved to the location and then the wind turbine is assembled. This process can be seen in Table B.2. The work times are listed as hours per turbine.

Table B.2: Turbine construction cycle

Activity	Equipment	Amount of equipment	Work time [h/turbine]
Transport of jack-up	Tugboat	2	48
Assembly of wind turbine	Jack-up	1	24

The installation of the cables consists of three distinct processes. These are the installation of the array cables, substation, the installation of the export cable, and the installation of the landing cable. These processes are further described in Table B.3. An important difference here is that the working times listed below are not per installed turbine but per km of specific cable.

Table B.3: Cable construction cycle

Activity	Equipment	Amount of equipment	Work time [h/km]
Substation installation	Jack-up	1	8
Dredging	Dredge	1	24
Route clearance	Anchor handling vessel (AHV)	1	3.24
Array-cable laying	plough-vessel	1	24
Support	Offshore support vessel (OSV)	1	24
Burial assistance	OSV	1	24
Rock transport	Barge	1	0.128
Rock placement	Barge	1	2
Export-cable laying	Plough-vessel	1	3.53
Rock transport	Barge	1	0.128
Rock placement	Barge	1	2
Landing cable laying	Plough-vessel	1	1.6
Support	OSV	1	4

B.0.0.2 Maintenance

Maintenance will take place during the operation of the wind farm. Usually, this is done with a smaller fleet than during construction and activities consist more of inspection and small fixes. A distinction between the two maintenance types can be made. Firstly, the regular preventive maintenance. Secondly, the irregular corrective maintenance. These are described in Table B.4 as work time per turbine per year. The fleet size should be large enough to handle the yearly preventive maintenance. In the case of irregular maintenance, a special vessel will be mobilized.

Table B.4: Maintenance cycle

Activity	Equipment	Amount of equipment	Work time [h/km]
Regular turbine inspection	OSV	1	60
Regular cable inspection	OSV	1	336
Regular substation inspection	OSV	1	180
Irregular inspection and repair	OSV	1	180
Replacement of nacelle	50% OSV & 50% jack-up	1	48
Replacement of blades	50% OSV & 50% jack-up	1	48
Replacement of small components	50% OSV & 50% jack-up	1	0.96

B.0.0.3 Decommissioning

Finally, at the end-of-life of the offshore asset, decommissioning needs to take place. During decommissioning, the foundations and turbines will be uninstalled but the cables will be left in situ [25],. The activities necessary for decommissioning can be seen in Table B.5 with work time per turbine.

Table B.5: Decommissioning cycle

Activity	Equipment	Amount of equipment	Work time [h/km]
Jack-up transport	Tugboat	2	24
Disassembly turbine	Jack-up	1	12

C

Appendix C: Sustainability scales

Table C.1: human health, exotoxicity, resource scarcity, carbon foodprint and total eco-cost in euro

Material type	cost to human health	cost of exotoxicity	cost of resource scarcity	cost of carbon footprint	total eco-cost
iron	0.02 €	0.02 €	0.06 €	0.12 €	0.22 €
high-alloy steel	0.11 €	0.33 €	0.29 €	0.62 €	1.35 €
low-alloy steel	0.03 €	0.11 €	0.08 €	0.31 €	0.52 €
copper	0.10 €	0.31 €	4.48 €	0.56 €	5.44 €
lead	0.06 €	0.37 €	1.67 €	0.25 €	2.34 €
aluminim	0.08 €	0.35 €	1.23 €	1.15 €	2.82 €
glass fibre	0.02 €	0.10 €	- €	0.16 €	0.28 €
carbon fibre	1.00 €	3.48 €	0.07 €	11.68 €	16.22 €
resin	0.00 €	0.03 €	0.71 €	0.30 €	1.04 €
polyethelene	0.04 €	0.05 €	- €	0.25 €	0.34 €
polypropylene	0.04 €	0.05 €	0.78 €	0.22 €	1.08 €
HFO	0.00 €	0.03 €	0.43 €	0.48 €	0.94 €
diesel	0.01 €	0.03 €	0.28 €	0.32 €	0.64 €

Table C.2: ReCiPe human health, exotoxicity, resource scarcity and CO_2/kg scales

Material type	ReCiPe human health [DALYs]	ReCiPe ecotoxicity [species loss/year]	ReCiPe resource scarcity [$]	CO2/kg
iron	1.19E-06	3.18E-09	0.05	0.9
high-alloy steel	9.36E-06	2.00E-08	0.37	4.69
low-alloy steel	3.34E-06	8.38E-09	0.04	2.31
copper	9.30E-06	1.93E-08	0.51	4.19
lead	8.48E-06	1.31E-08	0.20	1.89
aluminim	1.40E-05	3.22E-08	0.45	8.67
glass fibre	2.71E-06	5.67E-09	0.00	1.24
carbon fibre	1.39E-04	3.26E-07	8.86	87.82
resin	2.64E-06	6.98E-09	0.34	2.24
polyethelene	2.53E-06	6.26E-09	0.48	1.87
polypropylene	2.30E-06	5.51E-09	0.47	1.63
HFO	3.70E-06	1.05E-08	0.43	3.6
diesel	3.15E-03	1.10E-05	375.66	2.38

D

Appendix D: CAPEX costs

Table D.1: User defined cost variables

Variable	Cost [euro]
Steel price [euro/kg]	1.5
Export cable price [euro/m]	740
Array cable price [euro/m]	423
Electronics price [euro/kg]	10
Diesel price [euro/kg]	1.248
Heavy fuel oil price [euro/kg]	0.393
AHV rate [euro/day]	1000
OSV rate [euro/day]	3900
Barge rate [euro/day]	30000
Dredge rate [euro/day]	5000
Jack-up rate [euro/day]	100000
Plough-vessel rate [euro/day]	5000
Tug rate [euro/day]	1000